Carbon dot-based waterborne hyperbranched polyester nanocomposite

Highlights

Current chapter describes the fabrication, characterization and property evaluation of environmentally friendly waterborne hyperbranched polyester (WHPE)/carbon dot (CD) nanocomposites. In this investigation, CD was prepared from citric acid and glycerol in presence of cost free cow urine through a facile and one pot greener method. The prepared nanomaterials and the nanocomposite were characterized by different spectroscopic and analytical tools. Both CD and the nanocomposites exhibited excellent wavelength dependent down- and up- conversion fluorescence properties. Further, significant improvements in mechanical properties like tensile strength, Young's modulus, toughness and scratch hardness were observed for the thermosetting nanocomposites. Thermogravimetric analysis supported high thermostability while differential scanning calorimetry authenticated the glass transition temperature (T_g). The rheological study demonstrated shear thinning behaviour of the nanocomposite. The nanocomposite films exhibited good transparency in the visible range. Further, they were found to be highly biodegradable by *Bacillus subtilis* and *Pseudomonas aeruginosa* bacterial strains. They also possessed efficient self-cleaning ability as observed by photodegradation of formaldehyde and methylene blue under exposure of normal sunlight. Thus, this nanocomposite could be used as a promising eco-friendly material for different potential advanced applications.

Parts of this chapter are published in

1. **Hazarika, D.** and Karak, N. Photocatalytic degradation of organic contaminants under solar light using carbon dot/titanium dioxide nanohybrid obtained through a facile approach. *Applied Surface Science*, 376:276-285, 2016.
2. **Hazarika, D.** and Karak, N. Biodegradable tough waterborne hyperbranched polyester/carbon dot nanocomposite: Approach towards an eco-friendly material. *Green Chemistry*, 18(19):5200-5211, 2016

4.1. Introduction

Previous chapter addresses the development of functionalized graphene oxide (f-GO)-based WHPE nanocomposite as a heterogeneous catalyst with good mechanical and thermal properties. However, preparation of GO is a complex process and expensive, as well as it requires large amount of strong acid which is undesirable and hazardous. Further, functionalization of GO required one additional step and therefore longer time was required for fabrication of this nanocomposite. Thus, CD is aimed to use in this study for development of WHPE nanocomposite as they possesses many advantages like chemical inertness, lower cytotoxicity, photobleaching, etc. as mentioned in **Chapter 1** [1]. Further, they can be prepared from easily available bio-based raw materials through the simple and facile approaches [2-5]. CD particularly in a waterborne system is favored because of its easy preparative protocol, presence of large number of polar oxygeneous groups, nontoxicity, high water solubility, easy functionalizability, compatibility with other materials including polymer matrices and high biocompatibility [6]. Further, unison of quantum size of CD and good compatibility with the matrix may also result in transparent thermosets [7] which was lacked in case of f-GO-based WHPE nanocomposite. In addition, incorporation CD may introduce wavelength dependent photoluminescence (PL) properties [7] to the nanocomposite and optical emission in visible regions of CD in polyester matrix may be useful for photocatalytic applications [8]. Thus, the nanocomposite may able to remove the organic contaminants from the environment and possesses self-cleaning activity. The design and development of this type self-cleaning polymeric materials attracted significant interest over the past decades as they minimize the use of resources and generation of waste; and reduce energy consumption [9]. However, no work on polyester nanocomposite with CD is reported so far, though it has significant importance from the perspective of green chemistry. So, preparation and design of green WHPE/CD nanocomposites with competent performance are still urgent and significant. In literature, it was used as one of the interesting, useful and cost effective nanomaterials in epoxy, poly(ester amide), waterborne polyurethane, etc. [6, 7, 10, 11]. Mosconi *et al.* [10] reported the preparation of poly(urethane urea)/N-doped CD nanocomposite by an *in-situ* technique using DMF/THF dispersed CD. Authors also reported a poly(ester-amide)/N-doped CD nanocomposite for green oxidation of benzyl alcohol to benzaldehyde under visible light. The fabrication of waterborne polyurethane/CD nanocomposite with biocompatible

attributes was reported by Gogoi *et al.* [6]. De *et al.* [7] reported fabrication of a tough hyperbranched epoxy/CD nanocomposite by solution technique using ethanol as the medium. Thus, literature also remains silent on the use of CD in polymer system without using organic solvent.

Therefore, in the present investigation, CD was prepared through a facile *in-situ* and green preparative protocol using bio-based raw materials and incorporated into WHPE matrix for the first time through *in-situ* polymerization technique in absence of solvent and compatibilizing agents. Further to obtain highly tough, biodegradable and transparent polyester thermosets, the nanocomposites were modified with glycerol based hyperbranched epoxy (HBGE) in the presence of poly(amido amine) (PAA). In addition, these nanocomposites were also used for photocatalytic degradation of organic contaminants like, carcinogenic formaldehyde and model dirt, methylene blue under sunlight. It is therefore claim that the resultant nanocomposites would be exciting materials for achieving photoinduced self-cleaning, high performing biodegradable nanocomposite through a simple, greener and industrially acceptable protocol.

4.2. Experimental

4.2.1. Materials

Like previous chapter, in this study WHPE50 was used as the matrix for fabrication of the nanocomposite. Thus, the materials and method were used related to WHPE50 as described in **sub-Chapter 2B, sub-section 2B.2**.

Cow urine used for preparation of CD was collected from the nearest farm house of Tezpur University. Citric acid and glycerol used for CD preparation were the same grade as mentioned in **sub-Chapter 2A, sub-section 2A.2.1**.

Formaldehyde used for photocatalytic test was received from Merck, India with molar mass 30.03 g mol^{-1}, density 1.09 g cm^{-3} and boiling point 93-96 °C.

Methylene blue was procured from SDFCL, India and used here to check the self-cleaning ability of the nanocomposite.

Quinine sulphate was purchased from Sigma Aldrich, Germany and used in this study as the standard for measurement of quantum yield (QY) of CD.

Silica gel was procured from SRL, India and used here to coat the glass plate for self-cleaning test.

All other materials like solvents, HBGE, PAA, etc. used in this study were same as described in the previous chapter.

4.2.2. Characterization

The characterization and instrumentation methods for microscopic, spectroscopic, diffraction, mechanical and thermal testing were the same as mentioned in the previous chapter. In this study, the transmittance percentages of the nanocomposite films were evaluated using a UV-visible spectrophotometer. The visual transparency of them was checked by a pen mark naphthalene structure with thin films of thermosetting nanocomposite. Further, the optical color emission photos of CD and the nanocomposites were recorded in a UV light chamber (Test Master, India).

Further, PL spectra were recorded using a photoluminescent setup (PerkinElemer Singapore PTE Ltd., Singapore, Model LS 55) in an aqueous solution. The QY of CD was calculated using quinine sulphate as the reference. CD was dissolved in water while quinine sulphate was dissolved in 0.1 M H_2SO_4. Their PL spectra were recorded by fluorescence spectrophotometer at excitation wavelength 340, 380 and 520 nm. Then by comparing the integrated PL intensities (excited at 360, 380 and 520 nm) and the absorbance values (at the above mentioned wavelengths) of the CD with the references quinine sulphate, QY of CD was determined. The absorbance values of the solutions at the excitation wavelength were measured by an UV-visible spectrophotometer.

QY was calculated by using the formula as given below [2, 12]

$$Q_{CD} = Q_R \times I_{CD}/I_R \times A_R/A_{CD} \times \eta^2_{CD}/\eta^2_R \quad \text{.....(Eq. 4.1)}$$

where Q refers to the QY, I refers to the intensity of fluorescence, A is the absorbance at exited wavelength and η is the refractive index of the solvent used. The subscripts R used in the equation refer to reference (quinine sulphate).

4.2.3. Synthesis of CD

CD was synthesized from citric acid and glycerol in the presence of cost free cow urine. At first, equal amount (2.5 g) of citric acid and glycerol was dissolved in 15 mL distilled water. To the above mixture 30 mL cow urine was added. The reaction mixture was taken in a 100 mL conical flask plugged with a cotton cork and heated at a constant temperature of 150 °C for 4 h in a muffle furnace. After cooling to room temperature a dark brown product was obtained. This was dissolved in 20 mL of water and the residue was separated by filtration. Then the aqueous filtrate was centrifuged at 3000 rpm for 15

min under ambient conditions. The remaining water was evaporated at 60 °C by heating for 8-9 h to obtain highly fluorescent CD. The yield of the synthesized CD was found to be 70%.

4.2.4. Fabrication of the nanocomposite

WHPE/CD nanocomposites were fabricated by an *in-situ* technique without using any catalyst or organic solvent or neutralizing agent. The preparation of WHPE was a two stage single pot process. Like previous chapter, the first step of this fabrication process was same as the synthesis of pristine polyester as described in **sub-Chapter 2B, sub-sections 2B.2.1**. In the second step, required amount of glycerol and bis-MPA was added along with the desired amount of CD to the above reaction mixture. The reaction was carried out at 140 °C for 2.5-4 h (lower time was used for higher amount of CD to avoid gel formation). By following the same preparative protocol, three different nanocomposites were fabricated using 0.1, 0.5 and 1 wt% CD and denoted as PCD0.1, PCD0.5 and PCD1 respectively. Polyester in absence of nanomaterial was synthesized for comparison purpose and encoded as PCD0.

4.2.5. Preparation of the thermosets

The thermosets of this nanocomposite was obtained by following the same procedure as described in **sub-Chapter 2A, sub-section 2A.2.3.3**.

4.2.6. Biodegradation study

The biodegradation study of the nanocomposites was carried out using both gram-negative and gram-positive bacterial strains by following the same procedure as described in **sub-Chapter 2A, sub-section 2A.2.8**.

4.2.7. Self-cleaning test of WHPE/CD nanocomposite

The self-cleaning property of polyester nanocomposites was carried by determining the photocatalytic activity of them using formaldehyde as a model dirt compound. In a typical procedure, the nanocomposite films (0.7-1.0 g) were cut into small pieces and taken in 100 mL aqueous solution of formaldehyde (100 mg L^{-1}). Then the solution was exposed to the sunlight for photodegradation of the formaldehyde. The same experiment was done for all the nanocomposites. The change in concentration of the formaldehyde was monitored by determining UV absorbance intensity in the range of 300-400 nm for

specified time intervals (7-12 h) [13]. The photocatalytic activity of the films was calculated from the rate of change of concentration of formaldehyde with the exposure time. To study the recyclability of the films, the used pieces in the first cycle were taken out by normal filtration after obtaining the maximum extent of degradation of formaldehyde and the weight of the films was taken after drying. These dried films were further used for the next subsequent cycle.

4.3. Results and discussion

4.3.1. Synthesis of CD

CD was synthesized by carbonization of citric acid, glycerol and cow urine. CD was also formed from glycerol and citric acid in absence of cow urine. The role of cow urine is to enhance the florescence characteristics of CD. As it contains nitrogen containing compounds which influence the fluorescence characteristics. Thus, the synthesized CD exhibited strong fluorescence characteristics without using any additional passivating agent. Hence, it is one of the greatest advantages of using cow urine in the synthesis of CD [14]. However, the exact mechanism for the formation of the present CD was not known. In accordance to the literature reports [1, 2, 3] of carbonization of organic compounds, the following steps can be cited for the formation of CD. At first, the hydrolysis, dehydration and decomposition of the carbon resources had taken place in presence of acid catalyst (citric acid may also act as an acid catalyst). These results the formation of furfural aldehydes, ketones and other organic acids which may undergo subsequent polymerization and condensation to form some polymeric products. Finally these products aromatized and carbonized through different types of condensation and cycloaddition reactions. Finally, the desired CD was formed by a probable nuclear busting of the above products at their critical concentrations under the given conditions. Therefore, this one step synthesis of CD has a significant finding as the surface of CD was passivated by oxygen along with nitrogen. The synthesis of CD is shown in **Scheme 4.1**.

4.3.2. Characterization

The morphology of CD was accessed by TEM. TEM images (**Figure 4.1**) of CD confirmed the formation of spherical shape particles with average size less than 10 nm along with uniform distribution. The particle size distribution was represented by

histograms and obtained by counting about 100 particles. The histograms indicated that these are uniformly dispersed particles with size ranging from 1.5 nm to 7 nm. High magnification TEM image reflects that most of the particles possess well-resolved lattice fringes. The lattice spacing of CD was 0.32 nm which well agrees with the plane (002) spacing of carbon [1, 2, 15, 16].

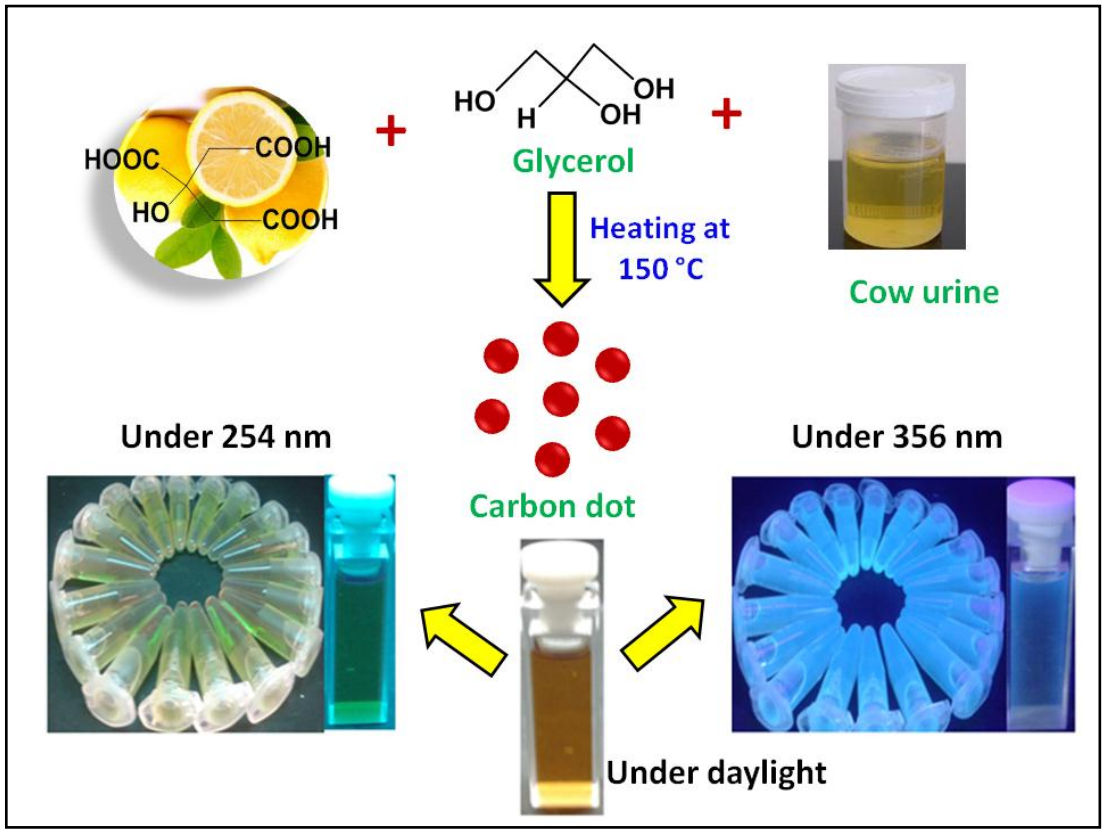

Scheme 4.1: Scheme for synthesis of CD

Elemental compositions of CD were determined from EDX data (**Figure 4.1**). The atomic and weight ratios of C, N and O of the CD were found to be 38.8:25.1:35.3 and 33.0:24.9:40.1. A minimum amount of potassium (1.83 wt% and 0.66 atomic %) was also present. Special elements like nitrogen and sulphur were present in CD without using any additional passivating agent due to the use of cow urine in the preparation.

The presence of different functional groups on the surface of CD was confirmed from FTIR spectroscopic studies (**Figure 4.2a**). In the FTIR spectrum of CD, the broad absorption band centered at 3436 cm^{-1} is attributed to the stretching vibration of -O-H, which implies the presence of large number of residual hydroxyl group on the surface of CD. The absorption band at 2923 cm^{-1} is due to -C-H symmetric stretching, 1731cm^{-1} and

1639 cm^{-1} correspond to stretching vibrations of -C=O and -C=C group respectively. The characteristic bands between 1000 ~ 1400 cm^{-1} are attributed to the asymmetric and symmetric stretching vibration of -C-O-C and band at 918 cm^{-1} is due to the presence of epoxy group. The presences of these functional groups bring excellent water solubility of CD. Moreover, the surface groups like oxygen and nitrogen can improve the stability of CD without any surface passivating agents or inorganic additives [1, 2, 8].

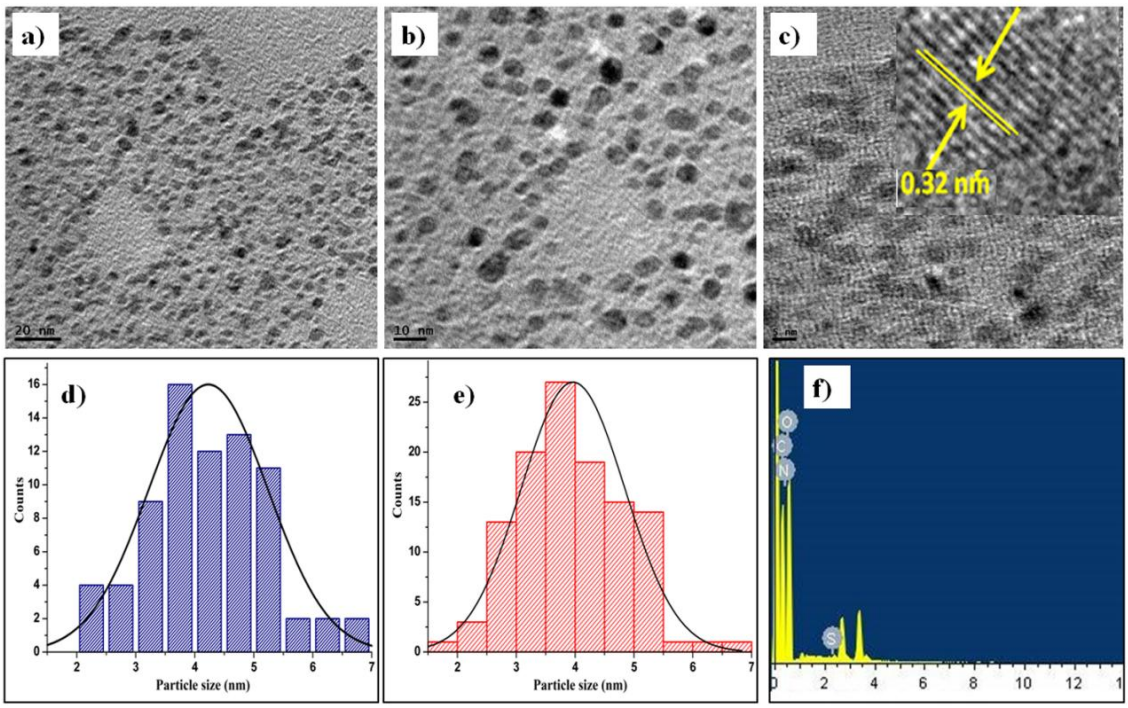

Figure 4.1: TEM images at different magnifications **(a)** 20 nm, **(b)** 10 nm, **(c)** 5 nm (inset: lattice fringe of CD), **(d, e)** particle size distribution histograms and **(f)** EDX pattern of CD

X-ray diffraction (XRD) pattern of CD is shown in **Figure 4.2b**. The CD showed a board peak centered at around 23° with d spacing between (002) planes is 0.37-0.39 nm. This board peak is due to highly disordered carbon atoms. This confirmed that CD is nearly amorphous in nature [2, 17].

Raman spectroscopy is also a powerful tool to identify the chemical state of carbon in CD. **Figure 4.2c** shows the Raman spectrum of the CD. The peaks centered at 1372 and 1618 cm^{-1} are attributed to the D band corresponds to disordered structure and G bands corresponds to sp^2-bonded C atoms in CD, respectively [18].

XPS was used to examine the elemental composition of CD. **Figure 4.3a** shows

XPS survey spectrum which reveals the presence of bands at around 285, 531, 398.5, and 164 eV correspond to C_{1s}, O_{1s}, N_{1s} and S_{1s} respectively. The atomic ratio of C/O/N/S is 63.64/ 33.22/1.54/ 0.59 as calculated from the survey spectrum. The C_{1s} core level band can be deconvoluted into five contributory peaks at 284.5, 285.6, 286.5 287.2 and 288.2 eV, which are attributed to the binding energy of C-C, C=C, C-N, C-O and C=O, respectively (**Figure 4.3b**). On the other hand O_{1s} band is deconvoluted into three peaks centered at 530.5, 532.0 and 533.0 eV corresponds to lattice oxygen, C=O and C-O-C/C-OH respectively **(Figure 4.3c)**. N_{1s} band can be deconvoluted to three peaks at 398.3, 399.7 and 401.4 eV attributed to the pyridinic, pyrrolic and quaternary N, respectively (**Figure 4.3d**). Similarly, the S_{2p} band consists of two peaks, centered at 162.7 eV and 167.5 eV corresponds to $S_{2P3/2}$ and $S_{2P1/2}$ respectively **(Figure 4.3e**) [19].

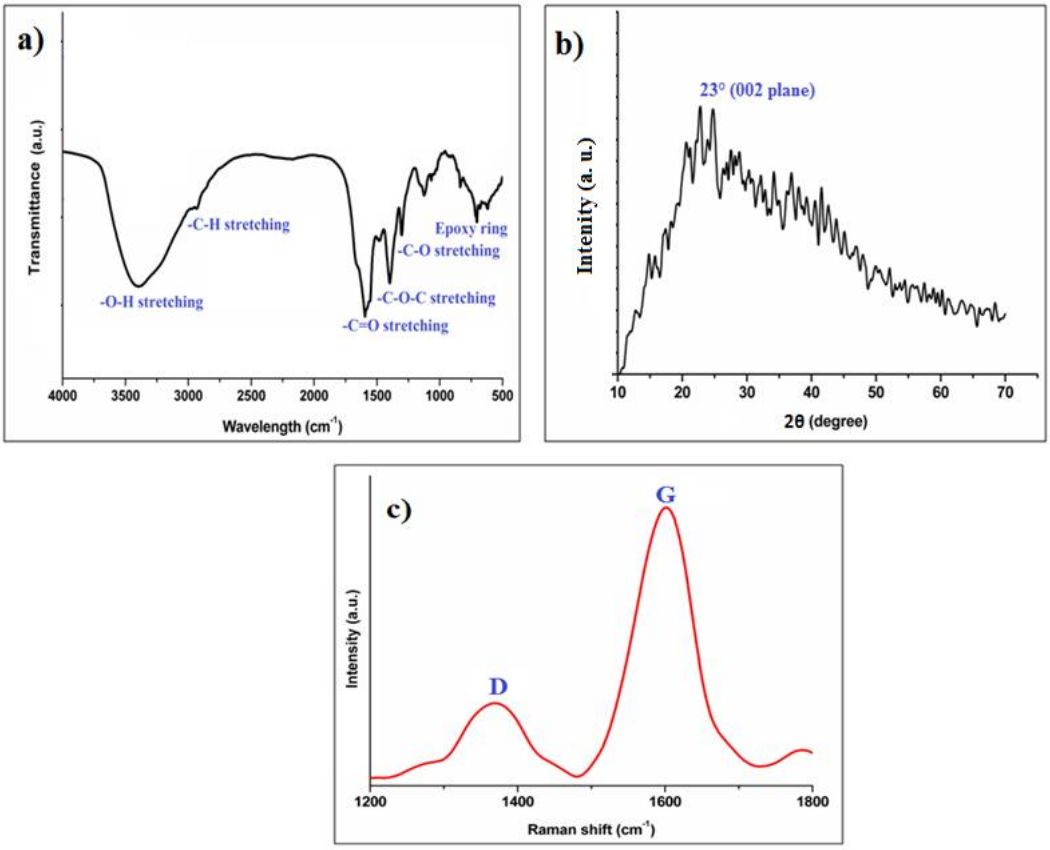

Figure 4.2: (a) FTIR spectrum, **(b)** XRD pattern and **(c)** Raman spectrum of CD

4.3.3. Optical properties of CD

The optical properties of CD in presence as well as in absence of cow urine, and other nanomaterials were studied by UV-visible and fluorescence spectral analyses. The UV spectrum (**Figure 4.4a)** of CD showed two characteristic absorption peaks at 235 nm

attributed to π-π* transition of aromatic C-C bonds, and a shoulder at 280 nm ascribed to n-π* transition of C=O bonds or other similar type groups [1, 2, 19, 20]. The aqueous solution of CD was brown in color under daylight but showed blue and green fluorescence under UV light at different wavelengths (**Figure 4.4a**). The maximum emission peaks for both CD were shifted from 420 to 560 nm with the increase of excitation wavelengths from 340 to 460 nm in the PL spectra (**Figure 4.4b**). It was also observed CD demonstrated excitation wavelength dependent down-conversion PL emission. This is due to the existence of different surface states and size dispersion of the nanomaterials. The QY of down-conversion of CD at 340, 380 and 520 nm were found to be 25, 15 and 5%, respectively.

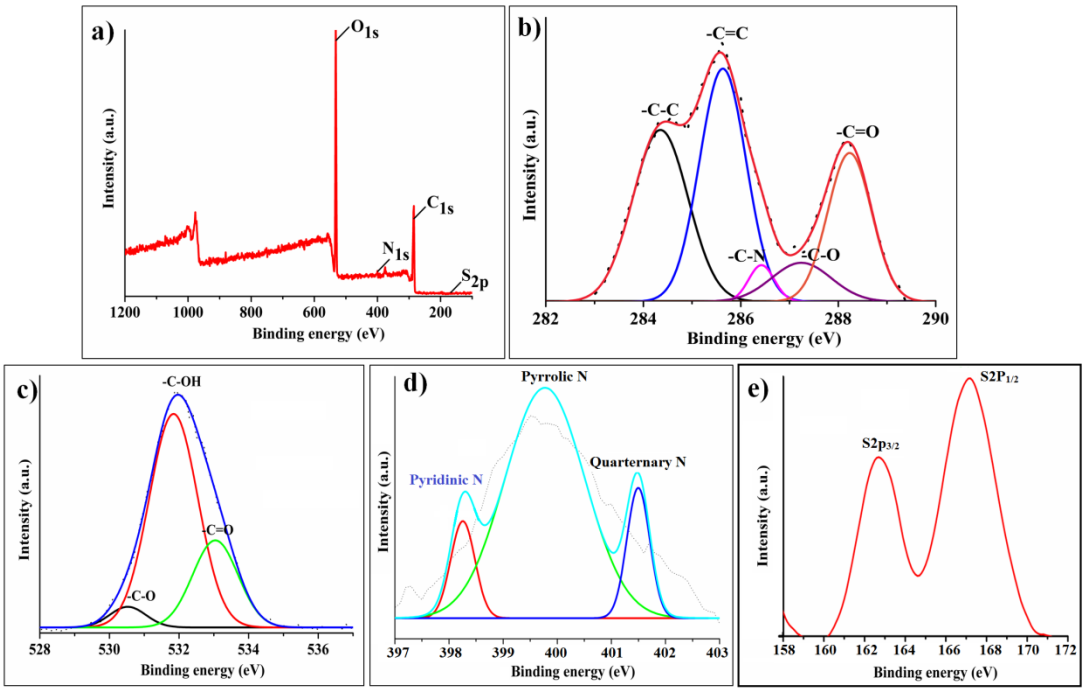

Figure 4.3: XPS spectra of CD **(a)** survey spectrum of CD with three major peaks of carbon, oxygen and nitrogen; XPS high resolution survey spectra of **(b)** C_{1s}, **(c)** O_{1s}, **(d)** N_{1s} and **(e)** S_{2p} regions of CD

They also possess excellent up-conversion fluorescence. With exciting the wavelengths from 650 to 800 nm, corresponding up-conversion emission spectra appeared from 420 to 525 nm **(Figure 4.4c)**. This characteristic may be attributed to the different emissive sites on each CD, distribution of different particle sizes of CD and the multi-photon active processes [1, 21]. The mechanism of the PL behavior of CD is not yet clearly established. The probable reasons for the PL behavior are due to the presence of different

sizes of particles and emissive traps existing onto the surface of CD. The difference in the position of emission peak is due to the size variation of CD. The intensity of PL also depends on the number of particles excited at a particular wavelength. In CD, the highest PL intensity was observed under excitation of 340 nm because at that wavelength the largest number of particles being excited. Another cause for the excitation dependent PL behavior of CD is surface chemistry. Further, the intensity of PL of CD increases with decreasing concentration of CD (**Figure 4.4.d**). This is due to increasing interactions among the different polar groups at higher concentration resulted agglomeration. The presence of different types of functional groups on the surface of CD may produce different emissive traps between π and π* of C=C. The self-passivated nitrogen and oxygen containing functional groups on CD surface may be responsible for the efficient PL by trapping excitons under excitation and the radiative recombination of those surface trapped excitons. CD on illuminating at a certain excitation wavelength a surface energy trap dominates the emission. The other corresponding surface state emissive traps become dominant as the excitation wavelength changes. Thus the mechanism of PL is controlled by both surface defects and size effects [1, 2, 3, 14].

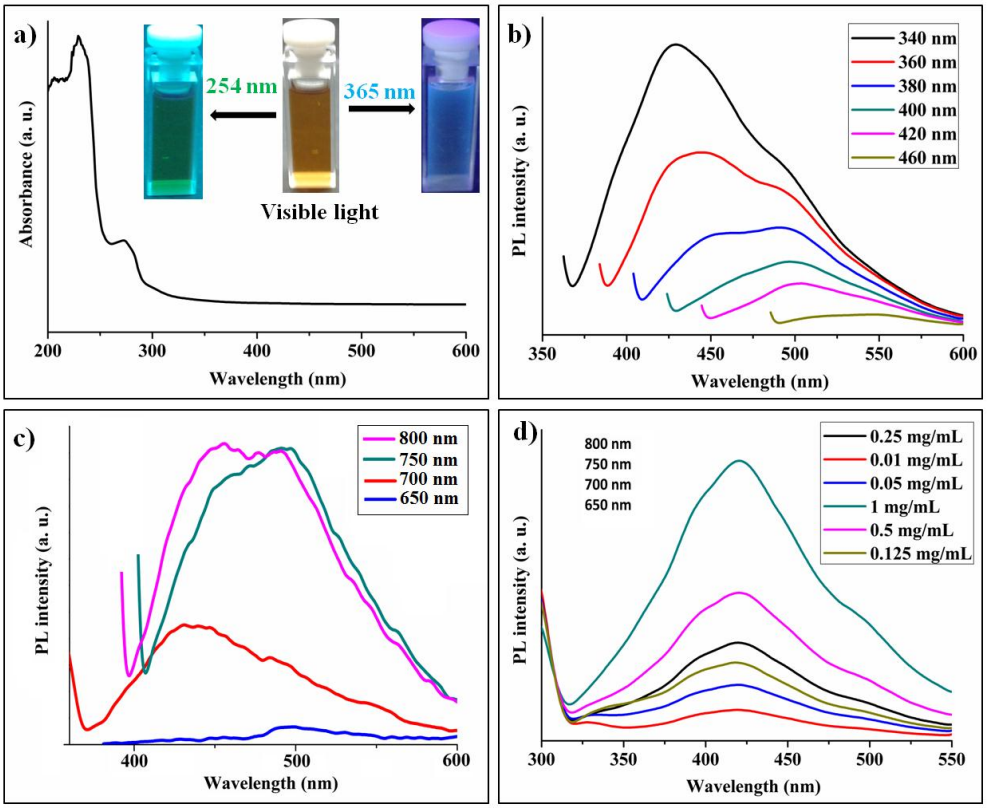

Figure 4.4: (a) UV-vis spectrum of CD, wavelength dependent **(b)** down- and **(c)** up-conversion PL spectra and **(d)** PL spectra of CD at different wt%

4.3.4. Fabrication and characterization of WHPE/CD nanocomposites

The nanocomposites of WHPE were fabricated by *in-situ* techniques using 0.1, 0.5 and 1 wt% of CD. The different oxygeneous functional groups of CD acquire an intrinsic tendency to interact covalently or non-covalently with WHPE as shown in **Scheme 4.2.** These types of interactions take part a vital role towards the homogeneous dispersion of CD in the polyester matrix. WHPE/CD nanocomposites were soluble (nanolevel) in most of the organic solvents like acetone, ethanol, THF, methanol, DMF, DMSO, DMAc, etc. and insoluble in ethyl acetate, hexane, xylene, toluene, etc. This is owing to the presence of bulky numbers of functionalities in the nanocomposites.

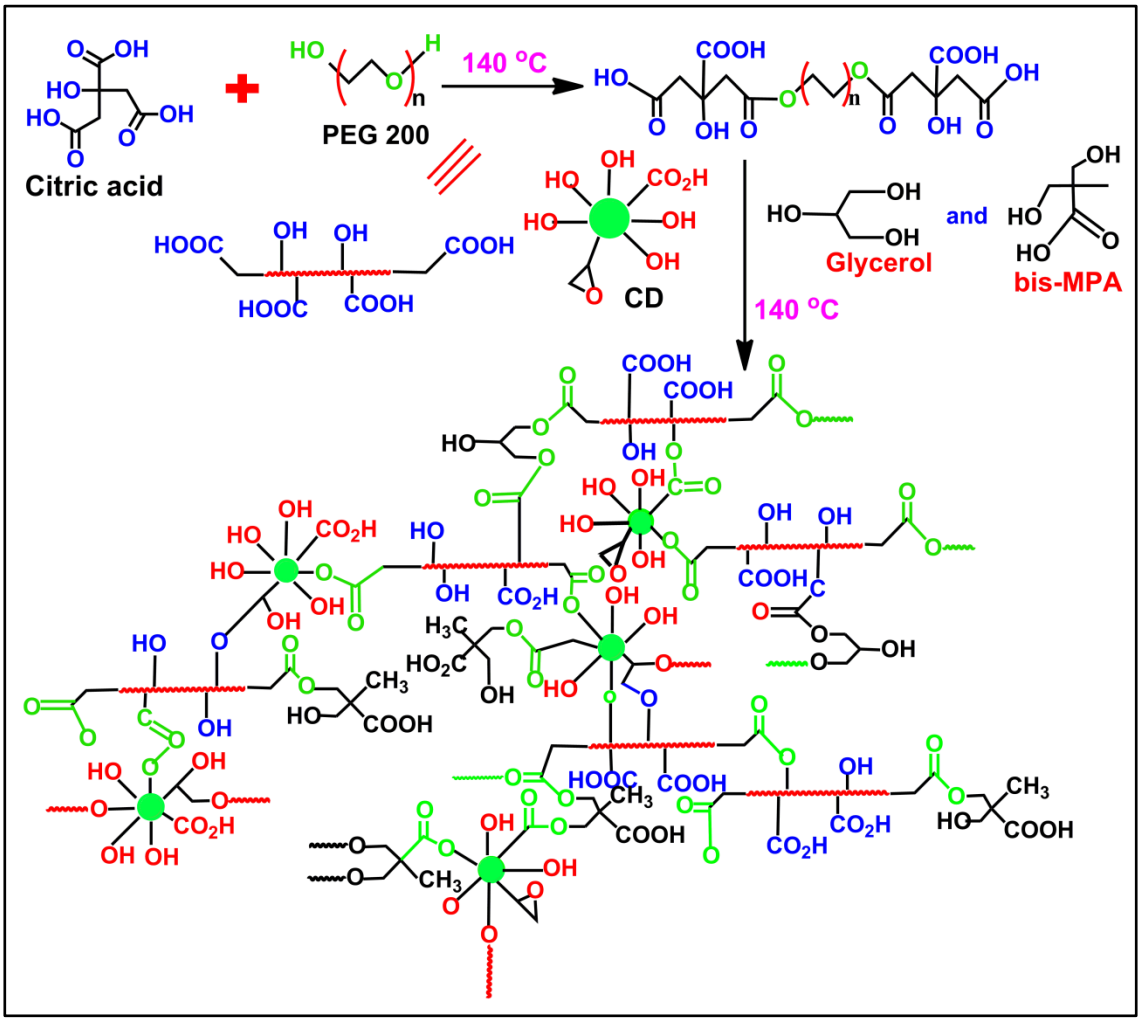

Scheme 4.2: Proposed scheme for fabrication of WHPE/CD nanocomposite

The presence of different functional groups in the nanocomposites was confirmed from FTIR spectra as shown in **Figure 4.5a**. From the FTIR spectra, it is seen that the absorption peaks are almost similar to pristine polyester except that the carbonyl

stretching vibration is shifted to lower frequencies (1724 cm^{-1}). The shifting of the peaks indicates the interactions of the polyester segments (-COOH and -OH) with CD through H bonding or other polar–polar interactions. The broadening of peak around 3400 cm^{-1} in FTIR spectra of nanocomposite compared to that of pristine polyester indicates hydrogen bonding between OH groups of WHPE and CD as well as strong interactions between them [6, 7, 11]. The formation of nanocomposite (PCD0.1) further weaken the crystallinity of the poorly crystalline CD as the intensity of the peak of bare CD at (23° in XRD pattern) was found to be diminished. The peak was also broadened and shifted to 25° in the nanocomposites (**Figure 4.5b**).

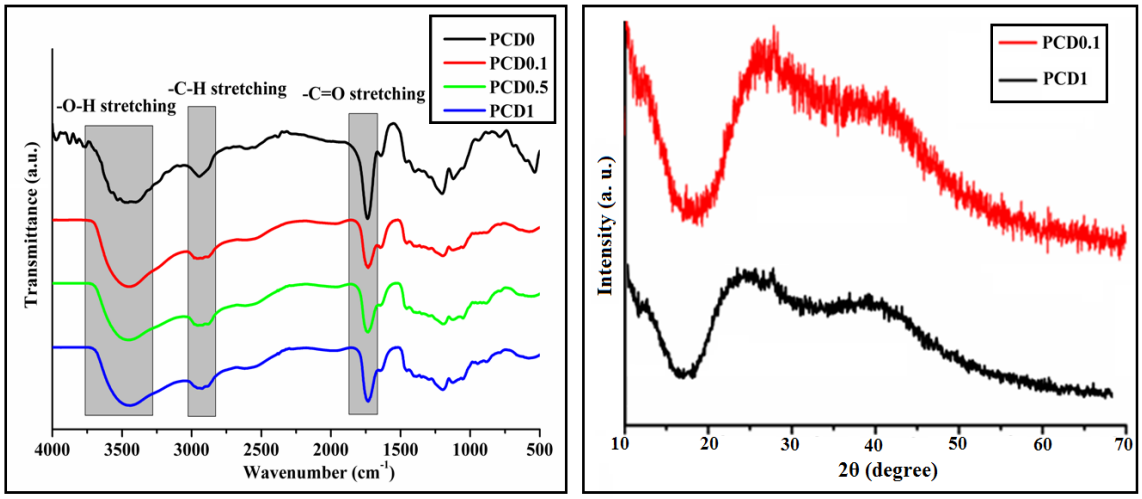

Figure 4.5: (a) FTIR spectra and **(b)** XRD patterns of the nanocomposites

This could be ascribed to disordered arrangement of the atoms caused by the strong interactions between polymer matrix and polar functionalities of CD. The poor crystallinity of CD, which was further decreased by the formation of nanocomposites, is also confirmed by the selected area electron diffraction (SAED) patterns of PCD0.1 (**Figure 4.6**). TEM images (**Figure 4.6**) of nanocomposite confirmed the excellent dispersion of CD in the polymer matrix showing that CD is well separated in the matrix without aggregation. CD was uniformly distributed even at higher loading which is confirmed from TEM images of PCD1. The well dispersion of the CD is due to the chemical binding with the polymer matrix through their large number of functional groups preventing agglomeration. Further, the interlayer spacing of CD increased after the formation of nanocomposite. This may be due to contribution of CD in chemical reaction which might further reduce the crystallinity of poorly crystalline CD [6, 7].

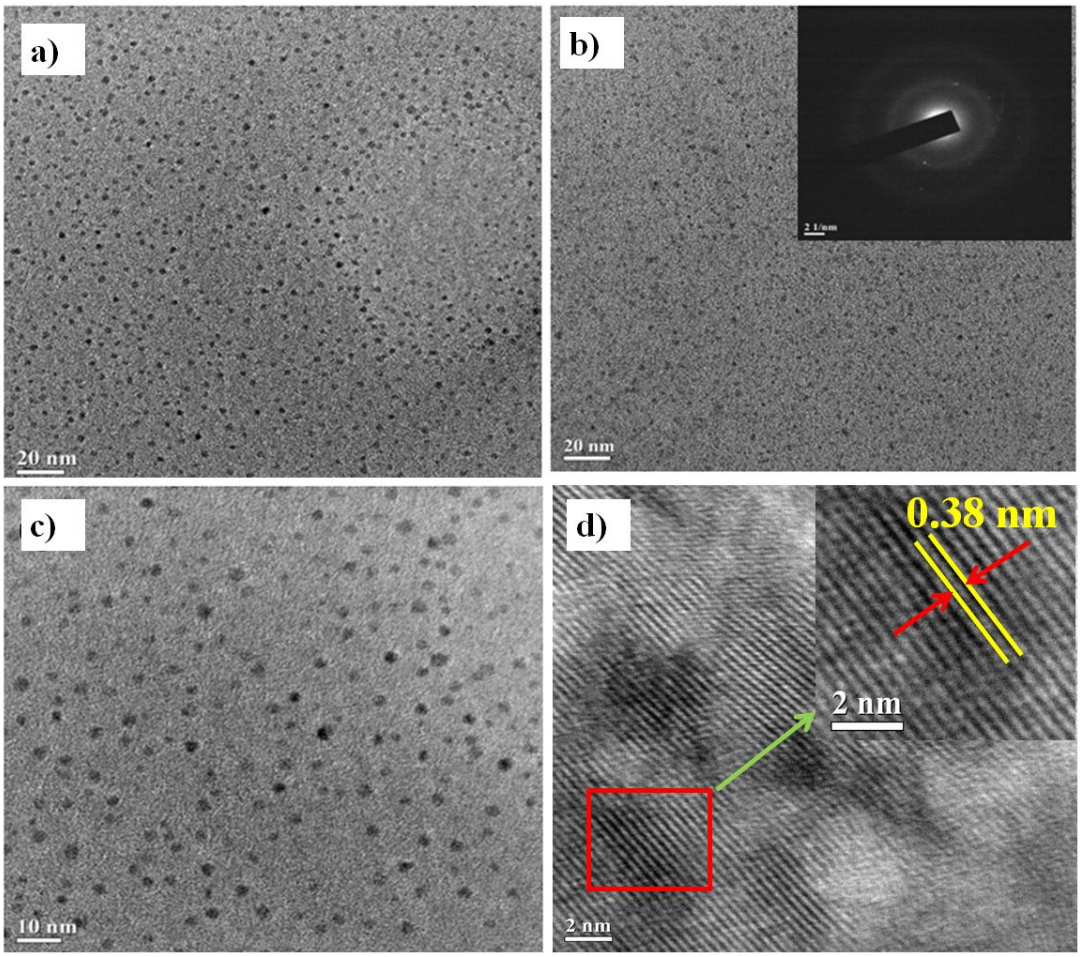

Figure 4.6: TEM images of **(a)** PCD1, **(b)** PCD0.1 (with SAED pattern as inset), **(c)** PCD0.5 and **(d)** lattice fringe

4.3.5. Rheological study

Rheological analysis was carried out to acquire information about the interaction between CD and polymer matrix since it is a vital factor in the enhancement of performance characteristics. The variation of shear viscosity of all the nanocomposites and pristine system before curing against time is monitored under single shear value and controlled stress and the results are shown in **Figure 4.7a**. It is seen that the viscosity remains almost constant with time though the viscosities of the nanocomposites were higher than the pristine system and the values increase with CD loadings. The enhancement in viscosity may be ascribed to higher interactions between CD and polyester that results in higher loading of CD. These interactions may moderately restrict segmental movements of the polymer chains [23]. Increase in viscosity caused by CNTs, organo clay, etc. have been reported, but the increase in viscosity at low loading of these is not as significant as that in our nanocomposite system [22-24]. These can be attributed

to the high surface area and large aspect ratio along with the presence of large number of interactive polar functional groups of CD which resulted in comparatively stronger CD-polyester interfacial interactions [22, 23]. However, the melt flow behavior of the nanocomposites was examined by the variation of shear viscosities with respect to temperature in the range of 25-75 °C at constant shear stress of 100 Pa (**Figure 4.7b**). It was noticed that the shear viscosity of the nanocomposites and the pristine system decreased with increase of temperature. This may be due to decrease in intermolecular H-bonding between CD and polyester segments and increase in kinetic energy of the different components present in the nanocomposites [23, 24]. In addition to these, the variation of shear viscosity as a function of shear rate for the pristine polyester and its nanocomposites was also monitored under constant temperature (**Figure 4.7c**). The shear viscosity of them decreased with increasing shear rate showing shear-thinning behavior signifying the formation of three-dimensional network structure [22, 25].

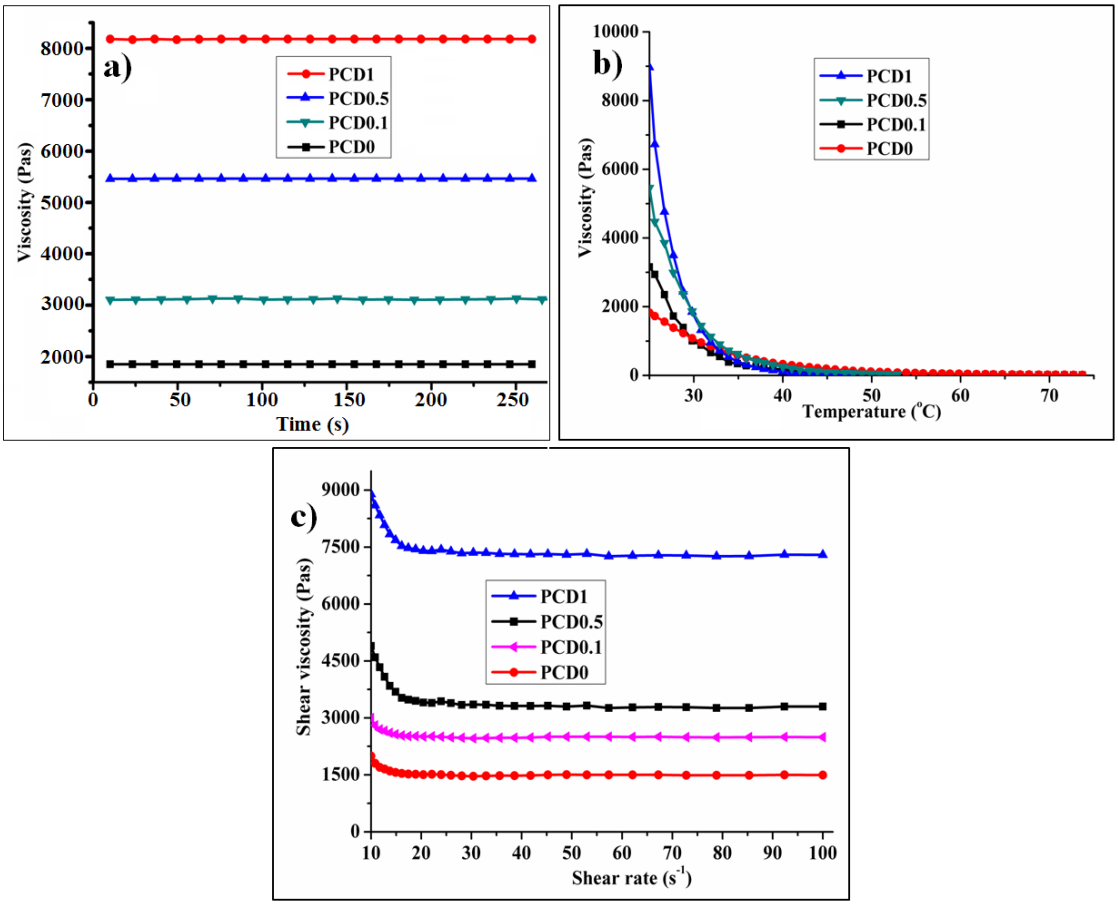

Figure 4.7: Variations of shear viscosity against **(a)** time at constant stress and temperature, **(b)** temperature under constant stress and **(c)** shear rate under constant temperature

The shear viscosity also increased drastically with the content of CD over a broad range of shear rates due to the above reasons.

The dynamic rheological behaviors of the WHPE/CD nanocomposites before curing were also examined by oscillatory experiments performed at an oscillatory stress of 20 Pa. The viscous and elastic characters of the pristine polyester and the nanocomposites before curing are characterized by loss modulus (G″) and storage modulus (G′) respectively [25, 26]. The viscoelastic properties of the pristine polyester and nanocomposites were examined by the frequency sweep experiment G′ and G″ were measured as a function of frequency (1 to 10 s^{-1}) under constant temperature (25 °C) and constant stress (20 Pa). The variations of G′ and G″ as a function of frequency for nanocomposites are shown in **Figure 4.8**. The variations of G′ and G″ of nanocomposite with the applied frequency revealed that both G′ and G″ values increase with the increase of frequency at different rates as well as with the loadings of CD. The sudden increase in the G′ and G″ values with frequency became prominent when the loading of CD increased from 0.1 to 1 wt%. The values of G′ compared to G″ over the entire frequency region were higher in magnitude due to the improvement of elastic behavior of the nanocomposites on incorporation of CD and a strong dependence of G' on interfacial energy over G″. In nanocomposites, the solid like elastic behavior, G″ < G′, dictated by the fusion of polymer-polymer, and polymer-nanomaterial interactions, signified the formation of a continuous network within the polymer matrix. With the loading of CD, the interactions between CD became prominent which ultimately led to the formation of permanent interconnected structures within the polymer matrix [25, 26, 27]. Further, the variation of G′ and G″ with respect to temperature (from 25 to 75 °C) under constant frequency (1 Hz) and controlled oscillatory stress of 20 Pa are shown **Figure 4.8c and 4.8d**. The values of G′ and G″ decrease with increase temperature which is due to the increase of kinetic energy and free volume of the polymer chains with temperature. This is in turn decreases the entanglement density and intra- and inter-molecular interactions within the polymer chains [26, 28, 29]. With the increase of loading of CD, both the values of G′ and G″ increase due to the same reasons.

4.3.6. Curing of the polyesters nanocomposite

The mechanism of curing of WHPE/CD nanocomposite, HBGE and PAA

hardener is a complex reaction owing to the presence of a large number of reactive functional groups such as -OH, -C=O, -COOH, epoxy, etc. in the system. Thus, a variety of reactions are possibly occurred between them and the plausible cross-linking reactions are shown in **Scheme 4.3**. The free -OH group of polyester and -NH_2 groups of hardener react with the epoxide groups of HBGE and CD. The transesterification reactions between ester (-O-C=O) and -OH groups can also occur. The hydrogen bonding between -C=O of hyperbranched polyester with -OH of HBGE and CD was formed.

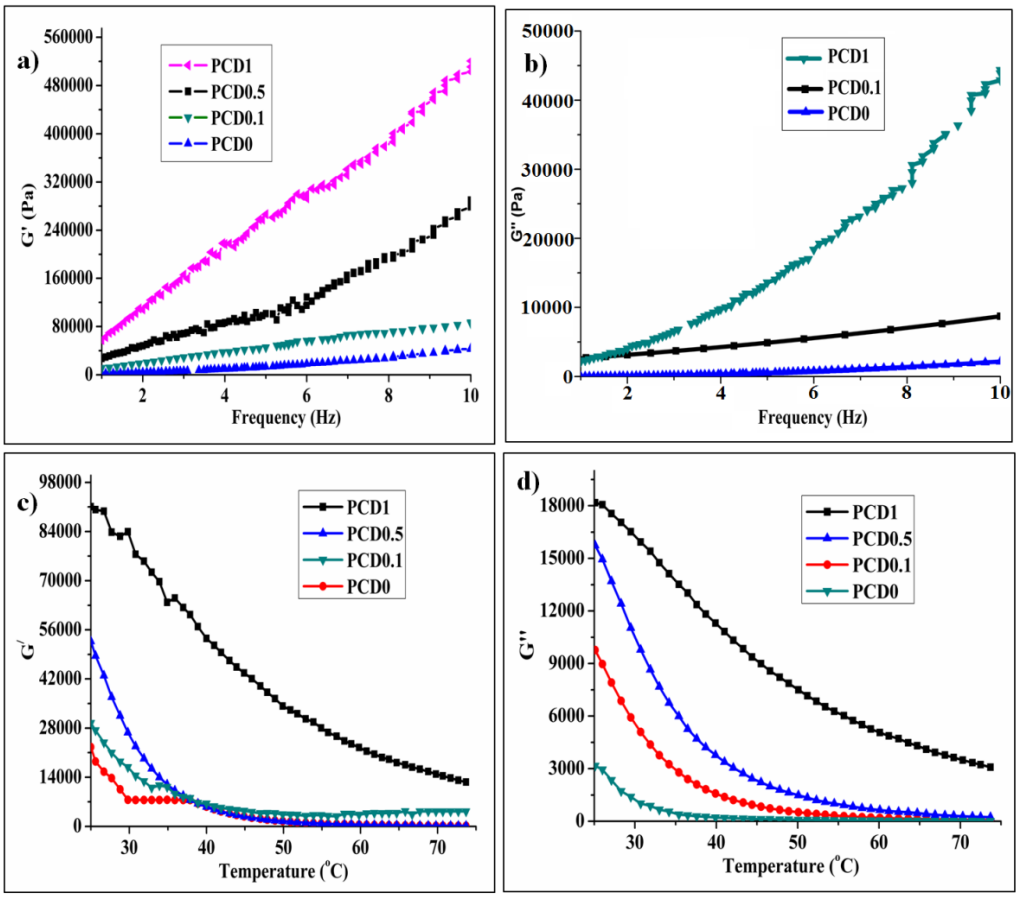

Figure 4.8: Variations of **(a)** G′ and **(b)** G″ with frequency and the variation of **(c)** G′ and **(d)** G″ with temperature for PCD0, PCD0.1, PCD0.5 and PCD1

The cross-linking reaction between free -OH groups of CD and polyester; and -NH_2 group of the hardener also takes place. Further, the hydroxyl-epoxy etherification reaction can also take place. The reactions among -COOH and -OH groups of the nanocomposite and CD, epoxide groups of HBGE and amino groups of the hardener would also be occurred. The rate of curing of nanocomposites

increased with the increase of CD loading and always higher than pristine system due to increase in the number of polar functional groups like -OH, epoxy, -C=O, -COO, etc. which took part in the cross-linking reaction. This also resulted in a strong interfacial interaction with WHPE. This is also attributed to the restricted mobility of the polymer segments along with the rheological properties, which helps in well-dispersion of CD and other components present in the nanocomposite systems. This homogenization of all the components facilitates to strong interactions and thus increased the rate of cross-linking reaction [7, 29-31]. The different curing times are required for curing of PCD0, PCD0.1, PCD0.5 and PCD1 to achieve nearly the same extent of curing as indicated by the swelling values (20-25%) of the resultant thermosets (**Table 4.1**).

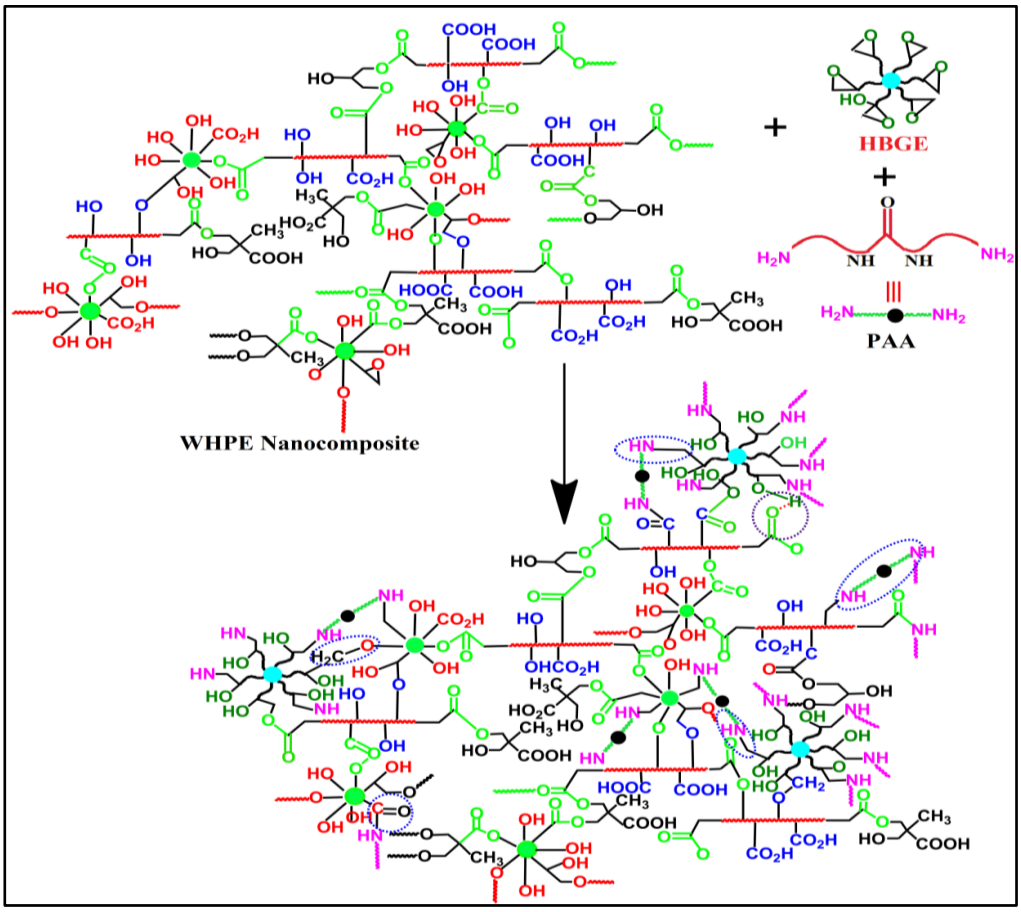

Scheme 4.3: Possible cross-linking reactions of WHPE/CD nanocomposite with HBGE and PAA hardener

The curing time is the time required to attain the desired swelling value (20-25%) of the thermosets. The specific gravity of the nanocomposite increases with the

increase of CD loadings (PCD0 = 0.95 ± 0.1 g cm^{-3}, PCD0.1= 1.08 ± 0.09 g cm^{-3}, PCD0.5 = 1.12 ± 0.08 g cm^{-3} and PCD1 = 1.16 ± 0.09 g cm^{-3}). This is owing to the increase in cross-linking density as measured by swelling value of thermosets of nanocomposite with CD loadings **(Table 4.1)**.

4.3.7. Optical properties of the nanocomposite

The optical properties of the nanocomposites were studied by UV-visible spectral analysis. The visual transparency was checked by structure of naphthalene covered with films of the pristine polyester and nanocomposite with different CD loadings (**Figure 4.9a**). The optical transparency of the nanocomposite films (thickness of about 0.3 mm) was also characterized by UV-visible spectroscopy and obtained optical transmittance spectra are shown in **Figure 4.9b**. The transparency of thermosets of polyester is not much affected after the formation of nanocomposites. **Figure 4.9b** showed that the transparency of all the nanocomposite films is good in the visible light range and the transmittance of these nanocomposite films is in the range of 95-70% (except at higher loading) at 800 nm.

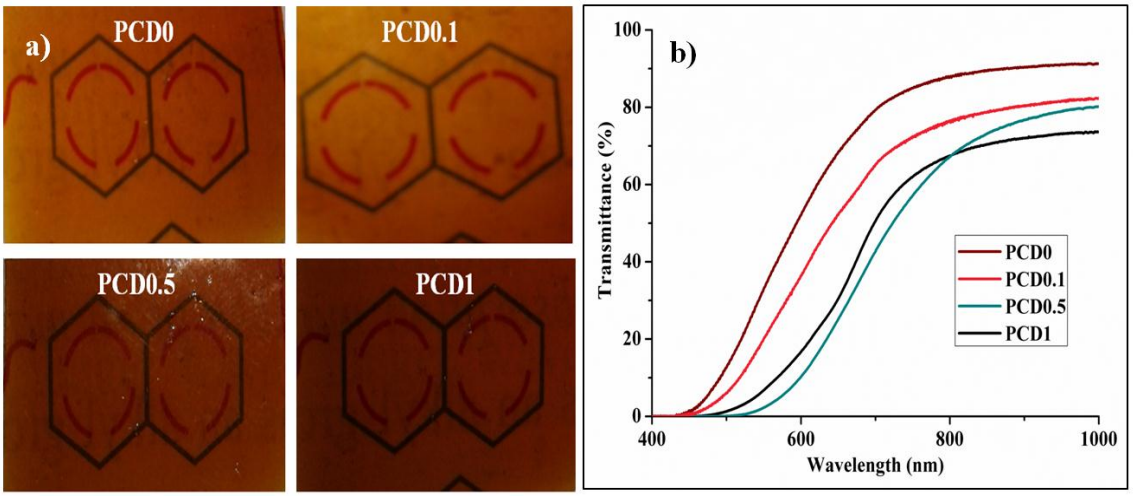

Figure 4.9: (a) Photographs for transparency and **(b)** transmittance spectra of PCD0 and its nanocomposites

In the UV region, the presence of CD has no effect on transmittance of the films. In the nanocomposites, the retention of high transparency is attributed to excellent dispersion ability of CD in the polymer matrix and the quantum size of it with large number of polar functionalities which took part in chemical cross-linking with HBGE and hardener

maintaining the nanosize in the thermosets [7, 31, 32]. Among the three nanocomposites, PCD0.1 showed the highest percent of transmittance of visible light and hence showed the highest transparency. The optical colors of nanocomposite films in the visible, shorter UV (254 nm) and longer UV (365 nm) regions are shown in **Figure 4.10a**. They are brown in color under visible light and changed into green under short UV light and to dark blue on exposure of long UV light. The color change at different wavelengths of UV light is due to the presence of different sizes of CD in the nanocomposites. CD with lower size get excited at short UV region and CD with higher size are excited at long UV region. The nanocomposites showed the maximum optical absorption in the UV region but extend with low intensity up to the visible range (**Figure 4.10b**). It is also owing to the π-π* transition of the conjugated -C=C and n-π* transition of the -C=C of graphitic structure of CD [7, 33]. The combination of low absorption in the visible range (400-800 nm) and high transmittance is a great advantage for self-cleaning property [34, 35]. Similar to CD, WHPE/CD nanocomposite also exhibited excitation wavelength dependent down- and up- conversion fluorescence properties which are monitored from PL spectra. An excitation wavelength dependent PL behavior was observed with shifting of the emission peak towards higher wavelength with increase in excitation wavelength (**Figure 4.10c**). This can be ascribed to the existence of different surface states and size dispersion of CD. With the increase of excitation wavelengths from 340 to 460 nm in PL spectra, the maximum emission peaks for CD were shifted from 430 to 560 nm. This confirmed the wavelength dependent down-conversion property of the nanocomposite. The up-conversion emission spectra appear from 430 to 530 nm upon exciting the wavelengths from 650 to 800 nm, (**Figure 4.10d)**. This feature may be ascribed to the different emissive sites and distribution of different particle sizes of CD as well as the multiphoton active processes [7, 36]. The quantum yield of PCD1 was found to be 17.2 using quinine sulphate as the reference according to **Eq. 4.1**, as measured from PL spectra on excitation at 380 nm wavelength, which was higher compared to CD (15). This is due to homogenous and uniform dispersion of CD in the polyester matrix in PCD1.

Further, the gloss value of polyester enhanced after formation of nanocomposite. The values increase with the increase of CD loadings from 0.1 to 1.0%. The obtained results are much superior to already reported polyester/ clay nanocomposite which showed gloss value from 40 to 60 with loading of 1-5 wt% nanoclay [22]. This improvement in results signified that the cured thermosets possess good dimensional

stability simultaneously with a smooth surface. Also with the increase of CD concentration a huge amount of light is reflected from the smooth surface, as a result gloss values increased [22, 33]. These results showed that high gloss is also possible to obtain by proper designing of waterborne system.

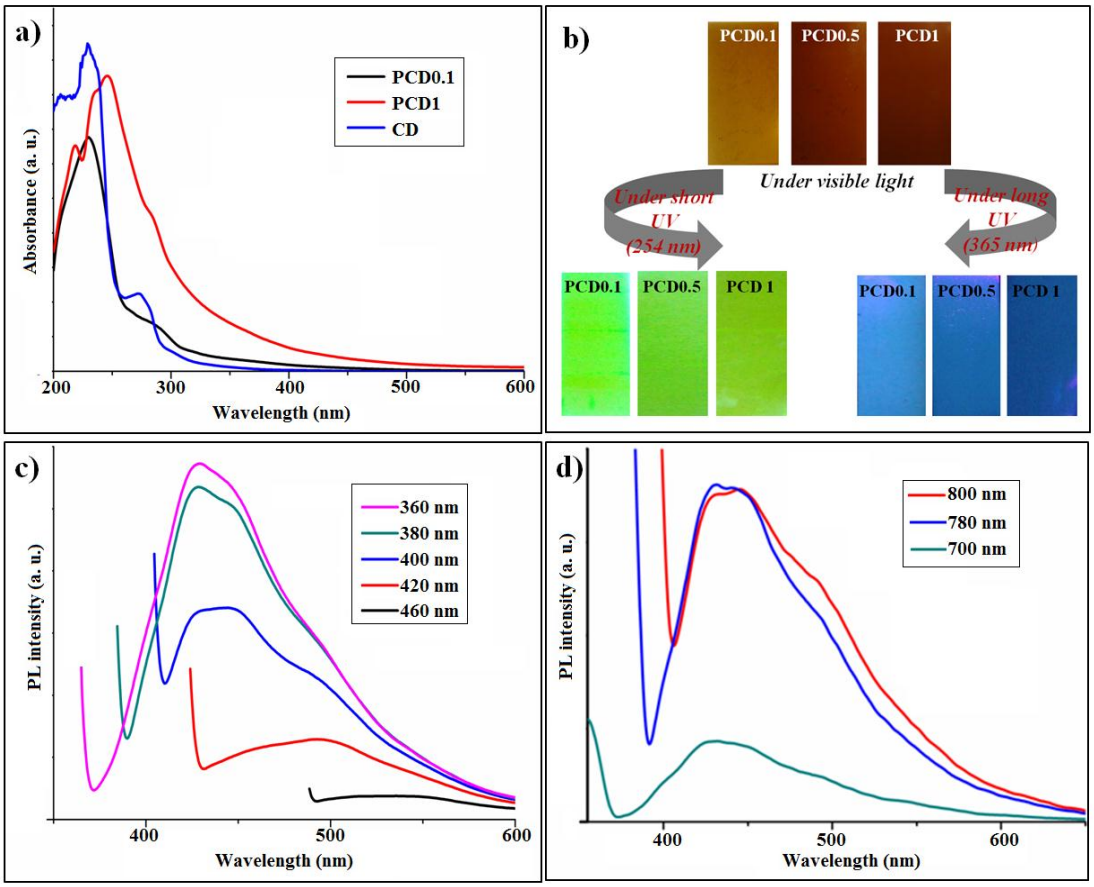

Figure 4.10: (a) UV-visible spectra of the nanocomposites, **(b)** films of PCD0.1, PCD0.5 and PCD1 under visible light, short UV (254 nm) and long UV (365 nm), wavelength dependent **(c)** down- and **(d)** up-conversion PL spectra of PCD1

4.3.8. Performance characteristics

The different performance characteristics of the three thermosets of WHPE/CD nanocomposite are listed in **Table 4.1**. The result of pristine system was also given for comparison purpose [30]. The stress-strain curves of them with various CD loadings are shown in **Figure 4.11a**. From the results, it is seen that outstanding enhancement of mechanical strength of nanocomposite compared to that of pristine one on incorporation of very minute amount of CD. It is evident that the addition of CD into the polymer matrix has a significant influence on the mechanical behaviors. The tensile strength

increases 2-6 times over the pristine system. The enhanced mechanical strength was ascribed due to homogeneous dispersion of CD in polymer matrix and strong interfacial interactions such as hydrogen bonding or some possible ionic interactions between the polymer matrix and CD. The polar functional groups (like hydroxyl, carbonyl, ether, epoxy, etc.) of CD took part in the chemical and physical cross-linking reactions with HBGE and PAA hardener. The strong interfacial interaction of the CD with the matrix helps to increase the rigidity, as reflected by the improvement of strength [7, 33, 37]. The obtained results are much better than the literature reported polyester/graphene oxide (GO) nanocomposite which showed increase in tensile strength from 32 to 54 MPa upon loading on 1-3 wt% GO [37]. The results are also far better than already reported polyester/clay nanocomposite (2.42- 6.28 on loading of 1-5 wt% nanoclay) [22]. On the other hand, elongation at break was started to decrease on incorporation of CD into the polymer matrix. This is due to the cause that the increasing crosslink density as stronger electrostatic interaction occurring in the nanocomposites which allowed lesser flexibility of the nanocomposite films. The large aspect ratio and the interaction between CD and the polymer matrix confine the movement of the polymer chains. These results are found to be superior to already reported polyester/GO nanocomposite which showed elongation at break (%) from 60 to 47 only on loading of 1-3 wt% GO [37]. However increase in the loading of CD also improved the toughness of the nanocomposite films which was measured by the area under the stress-strain curve.

Table 4.1: Performance characteristics of PCD0 and its nanocomposites

Property	**PCD0**	**PCD0.1**	**PCD0.5**	**PCD1**
Curing time (min)	300 ± 5	260 ± 4	200 ± 2	160 ± 3
Swelling value (%)	22 ± 2	22 ± 4	21 ± 3	20 ± 2
Tensile strength (MPa)	7.8 ± 3	16.1 ± 2	26.1 ± 3	47 ± 2
Elongation at break (%)	245 ± 2	201 ± 2	162 ± 4	140 ± 3
Toughness (MJ m^{-3})	17.8 ± 3	24.6 ± 4	32.8 ± 6	51.1 ± 2
Scratch hardness (kg)	4 ± 1	6 ± 0.5	7.5 ± 0.5	10 ± 0.5
Impact resistance (kJ m^{-1})*	>8.3	>8.3	>8.3	>8.3
Young's modulus (MPa)	243 ± 4	302 ± 4	347 ± 6	475 ± 3
Gloss (°)	94 ± 2	100 ± 3	107 ± 2	116 ± 2

**Maximum limit of the instrument*

This can be attributed to the stiffening consequence of CD, which has structure with aromatic carbonized core. As toughness of nanocomposites was significantly improved, the other mechanical properties like scratch hardness and impact resistance which were related to toughness were also enhanced A significant improvement in scratch hardness was observed in the nanocomposites, reinforced with 0.1, 0.5, and 1 wt% CD. The obtained values were superior to reported polyester/clay nanocomposite (4-6 kg on loading of 1-5 wt% nanoclay) [22]. With the inclusion of CD, the physical cross-link results in an effective network formation. The nanocomposites also exhibited high values of impact resistance. However, it was difficult to acquire the exact values as it crossed the limiting values of the used instrument. The Young's modulus values nanocomposites are shown in **Figure 4.11b** and it shows an increasing trend of modulus with CD loading.

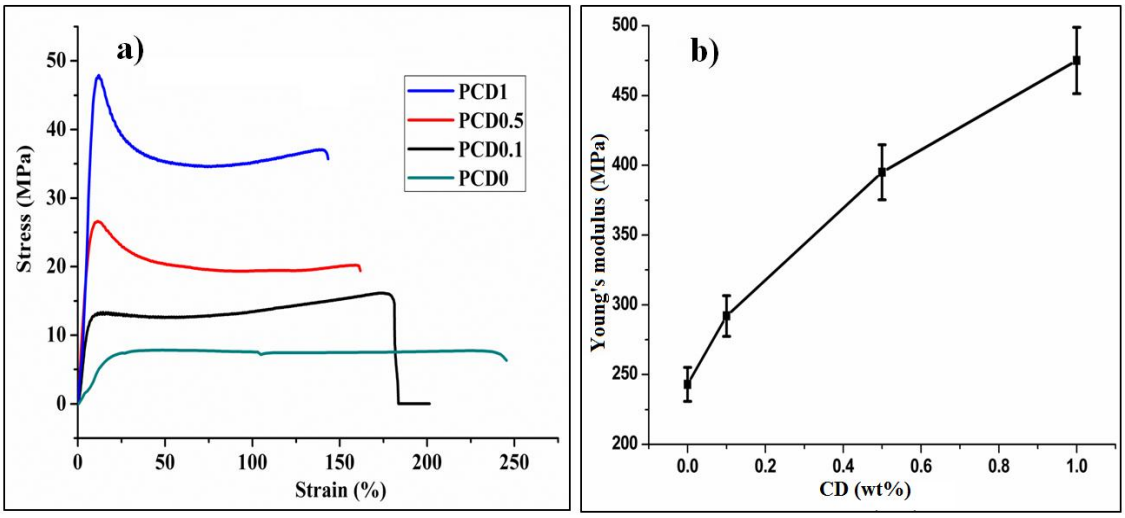

Figure 4.11: (a) Stress-strain profiles and **(b)** variation of Young's modulus with CD content for PCD0 and its nanocomposites

The obtained values are comparable to the literature reported values of polyesters (0.97-3.84, 33.3-51.0 and 0.19-1.10 MPa) [38-40]. This improved performance of the nanocomposites is due to strong interfacial interaction, excellent dispersion and nano scale interfacial domain structure. CD can provide strong interactions and stiffness in the polymer matrix due to the presence of large polar functional groups and its carbonized core structure, which play the critical role towards the superior mechanical properties of polyester nanocomposites. The presence of a carbonized aromatic structure of CD along with highly polar surface functionalities can lead to strong physicochemical interactions

of polyester, epoxy and the hardener which results in significant improvement of mechanical properties [33].

4.3.9. Thermal properties

TGA was carried out to evaluate the thermal stability of the nanocomposites. TG thermograms of them are shown in **Figure 4.12a**. The thermostability was enhanced after the formation of the nanocomposite with the loading of CD. The initial degradation temperature of the nanocomposite shifted to a higher temperature (234-265 °C) with CD content. The increased thermostability of the nanocomposites can be ascribed to high crosslinking density and secondary interactions imparted by CD with the polyester chains. The barrier properties of the CD are mainly responsible for enhancing the thermal stabilization of the nanocomposite. Furthermore, the presence of strong covalent and non-covalent interactions between the CD and polyester matrix enhances the thermal stability of the nanocomposites. Secondary interactions like polar-polar interactions and hydrogen bonding also play a crucial role towards the enrichment of thermal properties [7, 33].

The glass transition behavior of the nanocomposites was investigated by using DSC (**Figure 4.12b**). Pristine polyester exhibits glass-transition temperature (T_g) at around 49 °C as reported earlier [30]. With increasing CD loading in the nanocomposites, T_g of polyester increases gradually from 49 °C to 56°C. This increase in T_g indicates strong interactions between the polyester and CD such as hydrogen bonding which reduces segmental motion of the polymer chains.

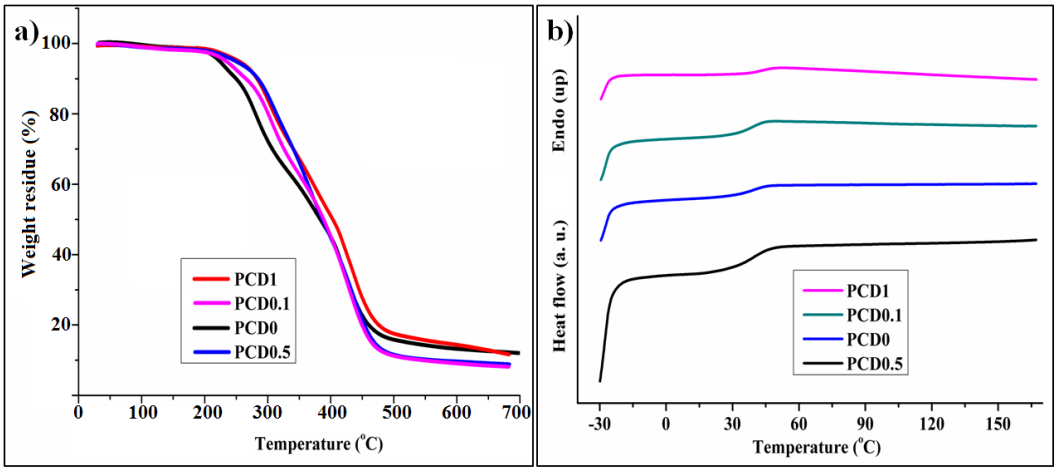

Figure 4.12: (a) TGA thermograms and **(b)** DSC curves of PCD0 and its nanocomposites

4.3.10. Chemical resistance

The chemical resistance of the thermosets of nanocomposites was carried out in different chemical environments viz. 0.5% aqueous sodium hydroxide, 10% aqueous hydrochloric acid, 15% aqueous sodium chloride, 20% ethanol and distilled water for 30 days under ambient conditions. The obtained results of chemical resistance (**Table 4.2**) indicated that the resistivity towards dilute aqueous NaCl solution, HCl acid and distilled water increases significantly after nanocomposites formation. However, the resistance towards alkali was not so good owing to the presence of alkali hydrolyzable ester group. But, after formation of nanocomposite with 0.1-1 wt% CD loading, this alkali resistance of the polyester thermosets was enhanced. As CD loading increases, the resistance towards all other media increases which may be due to compact and cross-linked structure of the nanocomposites where CD is bonded to the polyester matrix, HBGE and PAA. Due to these, different ions or species present in different media cannot be easily penetrated the surface and thereby increasing the resistance [22, 29].

Table 4.2: Change in weight (%) of the PCD0 and its nanocomposites in different chemical media

Chemical media	PCD0	PCD0.1	PCD0.5
0.5 wt% NaOH	4.5	3.5	2.1
10 wt % HCl	0.4	0.4	0.2
15 wt % NaCl	0.02	0.02	0.02
20 wt % EtOH	2.3	1.5	0.9

4.3.11. Biodegradation study

Polyesters owing to the presence of hydrolysable ester bond in their polymeric chain are prone to microbial attack [22, 30]. The thermosets of nanocomposite were directly exposed to gram-negative and gram-positive bacterial strains. The bacterial growth curves as measured by OD of degraded polyester nanocomposite films with time are shown in **Figure 4.13 and 4.14.** The growth curve for pristine system as reported earlier is shown for comparison purposes. WHPE after the formation of nanocomposite had shown high biodegradation rate as compared to the pristine system, after four weeks.

The growth of both the bacterial strains was increased with increasing bacterial exposure time. However, the obtained results of biodegradation evidently indicated the difference in bacterial growth for gram-negative and gram-positive bacteria. Gram-negative bacterial strain showed higher rate of biodegradation compared to the gram-positive bacteria because of their different cell structures. The presence of terminal hydroxyl groups in CD may be responsible for this enhanced biodegradation behavior after nanocomposite formation. The factor that enhances the hydrolysis propensity of polyester finally controls the degradation. CD in the nanocomposite plays a catalytic role in hydrolysis of the ester groups. In the nanocomposites, CD is homogeneously dispersed in the polyester matrix and the hydroxyl groups of CD start heterogeneous hydrolysis of the polyester matrix after absorbing water. As the loading of CD increases the rate of hydrolysis of ester bonds also increases which results higher rate of biodegradation [22, 29].

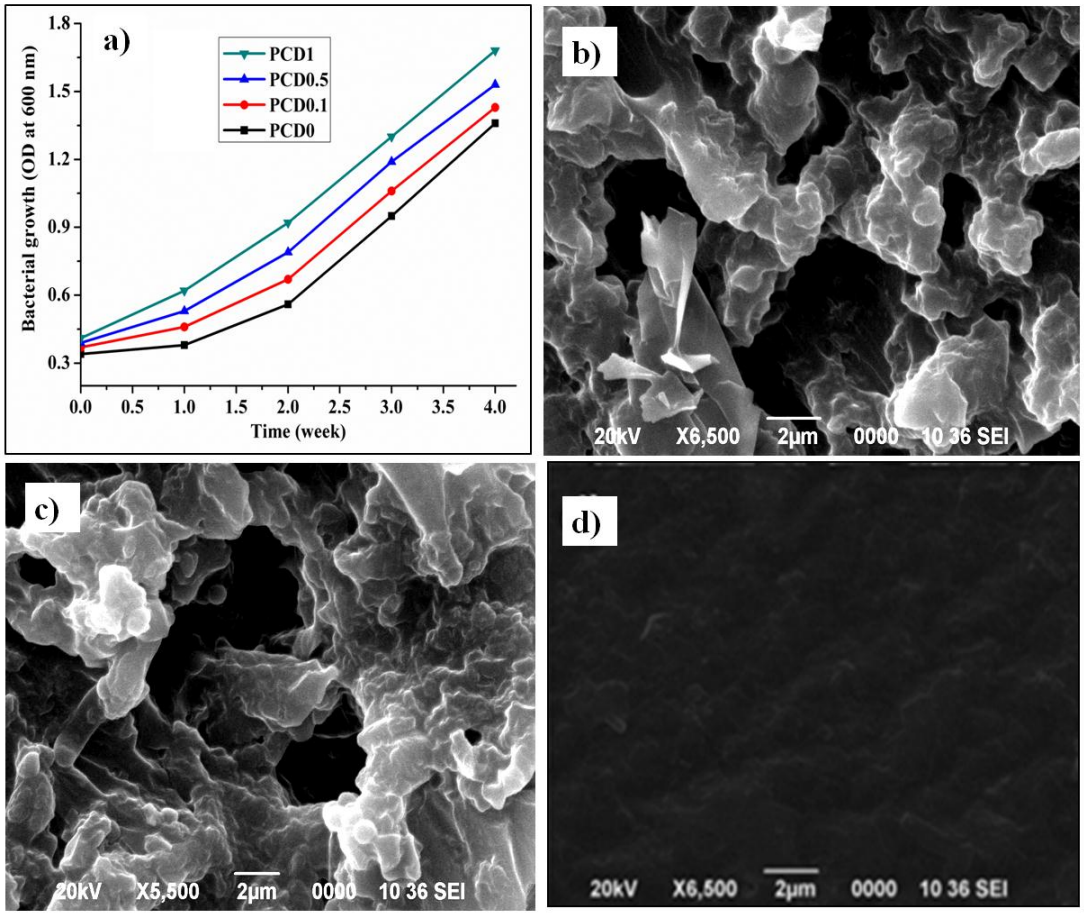

Figure 4.13: (a) Growth curves and **(b-d)** SEM images of degraded films of PCD0.5, PCD1 and control respectively by *Pseudomonus argeunosa* bacterial strain

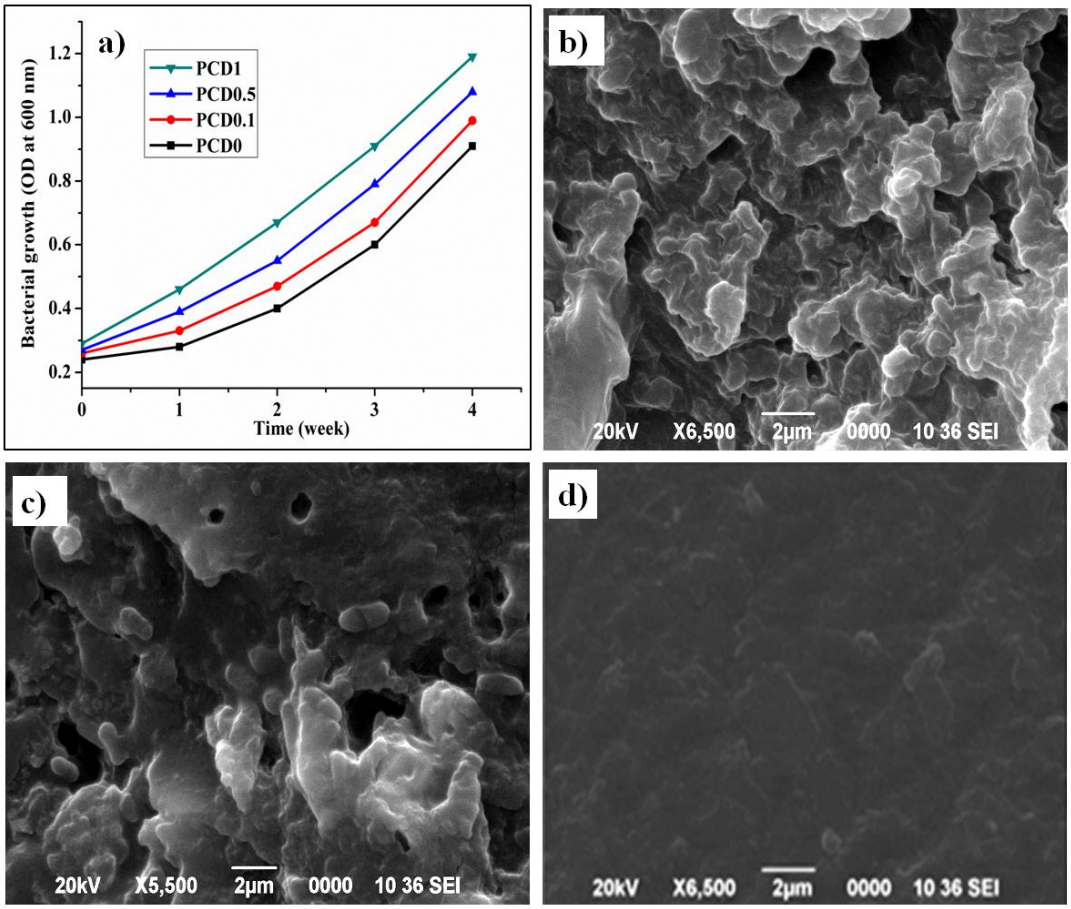

Figure 4.14: (a) Growth curves and SEM images of degraded films of **(b)** PCD0.5, **(c)** PCD1 and **(d)** control by *Bacillus subtilis* bacterial strain

Among all the thermosets of WHPE/CD nanocomposites, PCD1 showed the highest rate of biodegradation as it contains the highest content of CD. The representative SEM micrographs of PCD0.5, PCD1 and control (film without bacterial medium) after four weeks of bacterial exposure further support the biodegradation and the images are shown in **Figure 4.13** and **4.14.**

4.3.12. Sunlight induced self-cleaning property of WHPE/CD nanocomposite

To achieve self-cleaning, a film either be superhydrophilic or be able to induce photocatalytic oxidative decomposition of dirt on the surface or both [35, 41]. To evaluate the photocatalytic oxidative decomposition performance of nanocomposites films, formaldehyde was selected as model organic dirt. Photocatalytic degradation of formaldehyde was studied by all the three thermosets of nanocomposites under sunlight. The nanocomposite films were chopped into tiny pieces to increase the surface area. The plot of optical absorbance against wavelength for the degradation of formaldehyde at

different times for PCD1 is shown as a representative in **Figure 4.15a**. The degradation of aqueous formaldehyde solution based on its concentration changes with time was monitored by UV absorbance and shown in **Figure 4.15b**. The photocatalytic activity of the reused films of the nanocomposites was checked for another two times (**Figure 4.15c**). The results authenticated no significant decrease in photocatalytic activity of the films. The nanocomposite demonstrated considerable degradation of formaldehyde in the presence of sunlight. Among all the thermosets of nanocomposite, PCD1 efficiently degraded formaldehyde with 7.5 h sunlight exposure with good reusability. Further, the fitting plots of ln (C_0/C) with time are shown in **Figure 4.15d.**

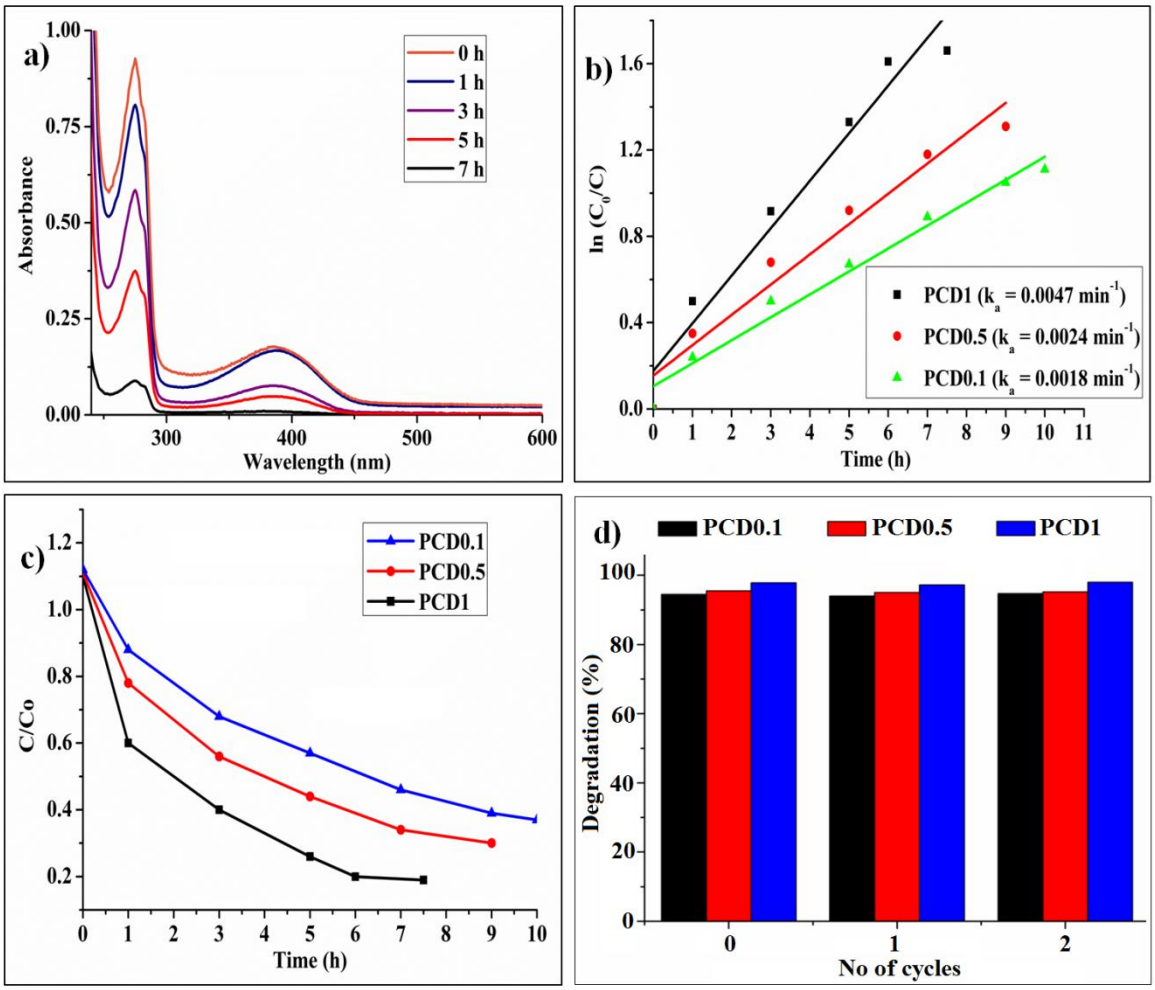

Figure 4.15: (a) Time-dependent UV absorption spectra of formaldehyde solutions during sunlight irradiation, **(b)** degradation curves of the aqueous solutions of formaldehyde by the nanocomposite films, **(c)** fitting degradation kinetic curves and **(d)** photocatalytic efficiency of nanocomposite

On the basis of previous studies, the degradation of formaldehyde can be ascribed to a pseudo-first-order reaction with a simplified Langmuir-Hinshelwood model:

$$\ln(C_0/C) = k_a t \quad \text{..... (Eq. 4.2)}$$

where k_a is the apparent first-order rate constant [35, 41, 42].

The degradation of formaldehyde produces water and carbon dioxide [36]. On the basis of the kinetic plot, PCD1 has the highest rate constant as compared to the other nanocomposites.

Further, the self-cleaning property of nanocomposites is also examined by degradation of methylene blue as model dirt on silica coated film under sunlight by visual means. The nanocomposite films decolorize the color of methylene blue. For better comparison, half part of a glass slide is coated with silica and other half is coated with silica in the presence of nanocomposite. Then the films were dipped in aqueous solution of dye and exposed to sunlight. With exposure time the change in color of the films was recorded at different times as shown in **Figure 4.16**.

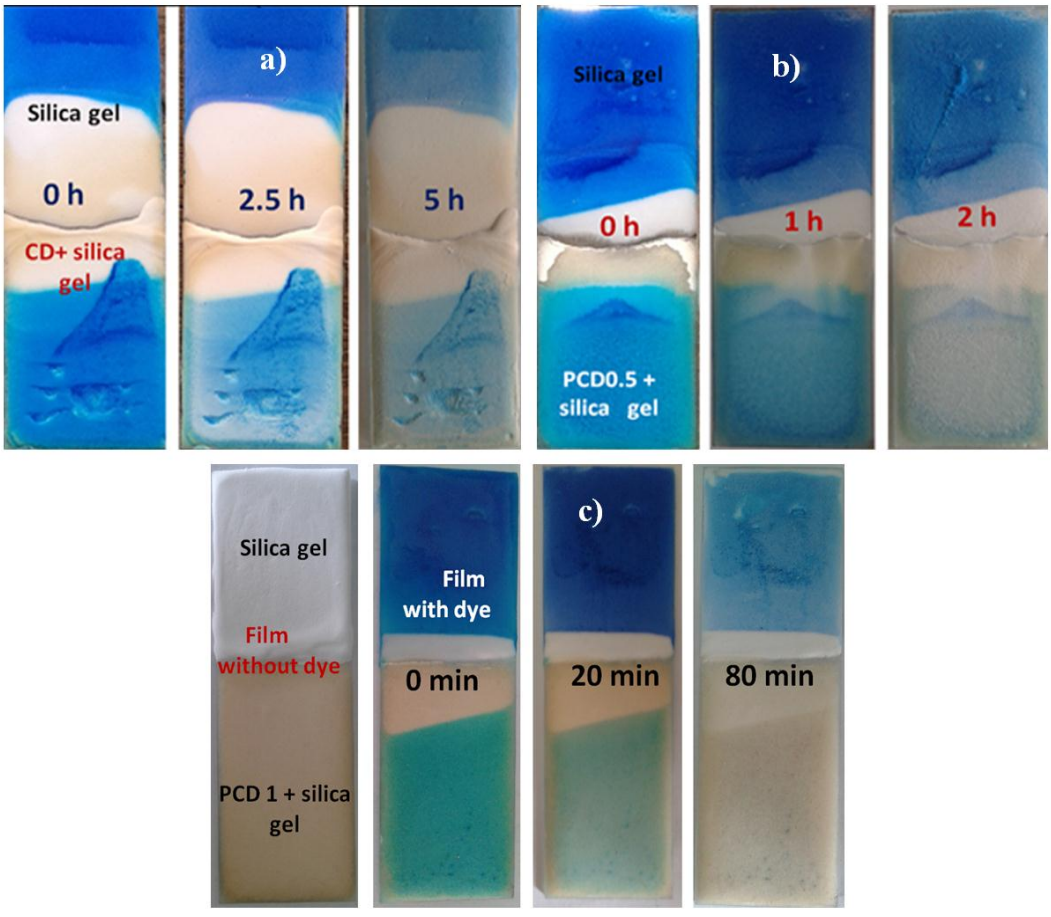

Figure 4.16: Photographs showing the discoloration of methylene blue by **(a)** CD, **(b)** PCD0.5 and **(c)** PCD1

The photographs illustrate the decolorization of model dirt over a period of 80 min by PCD1 and 120 min by PCD0.5. The results clearly indicated self-cleaning property of the nanocomposites is dose dependent and it increases with the increase in the concentration of CD. Thus, it can be utilized as a thin film for self-clean surface. On exposure of sunlight, electrons and holes are generated from CD. These electron and hole pairs generate oxygen radicals ($\bullet O_2^-$) from O_2 and hydroxyl radicals (•OH) from water which subsequently cause degradation of formaldehyde remained adsorbed on the surfaces of CD. A proposed photodegradation mechanism is schematically shown in **Scheme 4.4** based on other reported CD/metal and/or metal oxide nanoparticles by utilizing the up-conversion fluorescence property of CD.

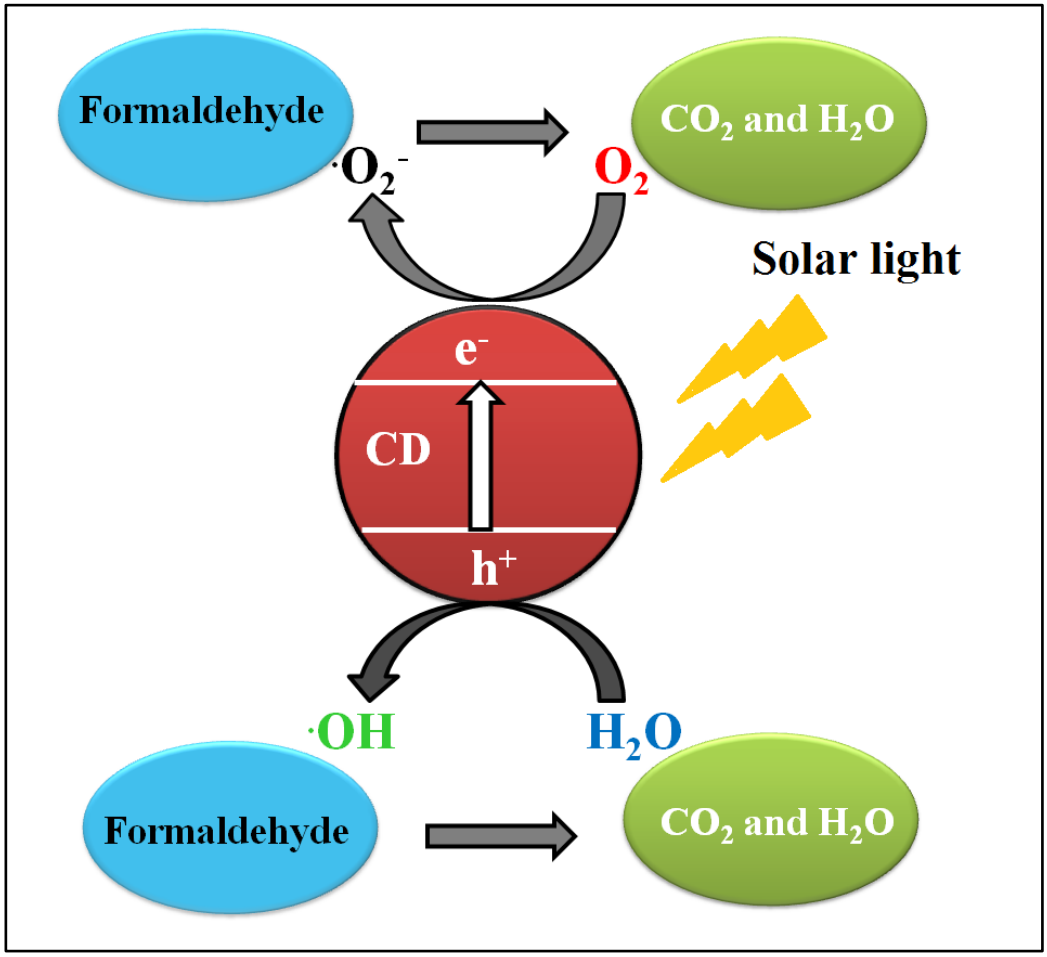

Scheme 4.4: Proposed mechanism for formaldehyde degradation

4.4. Conclusion

The present study demonstrated a green, facile and environment friendly *in-situ* fabrication of the high-performance waterborne hyperbranched polyester/CD

nanocomposites for the first time. The preparative method does not use any catalyst as well as organic solvent and it is technically possible for large-scale fabrication of such high performing nanocomposites. Thus, the employed method opens up new opportunities for utilizing the inimitable properties of CD for a wide range of applications. Further, use of bio-based raw materials for preparation of CD and polyester; and hence nanocomposites bring eco-friendliness and sustainability to the fabricated nanocomposites. The results showed that incorporation of CD drastically improved the mechanical, rheological, thermal and optical properties of polyester nanocomposites. The films of nanocomposites exhibited self-cleaning property as found for photocatalytic degradation of formaldehyde. The excellent mechanical properties with good transparency and fluorescent behavior provide this material highly interesting in optical devices like LED, UV light detection systems, etc. Thus, these nanocomposites may be used as high performance materials for diverse applications. Moreover, this unique approach may be extended to form other nanocomposites with multifaceted functional properties and thus, opens up enormous opportunities for exploiting them for a wide range of applications.

References

[1] Alam, A. M., Park, B. Y., Ghouri, Z. K., Park, M., and Kim, H. Y. Synthesis of carbon quantum dots from cabbage with down- and up-conversion photoluminescence properties: Excellent imaging agent for biomedical applications. *Green Chemistry,* 17(7):3791-3797, 2015.

[2] De, B. and Karak, N. A green and facile approach for the synthesis of water soluble fluorescent carbon dots from banana juice. *RSC Advances,* 3(22):8286-8290, 2013.

[3] Yin, B., Deng, J., Peng, X., Long, Q., Zhao, J., Lu, Q., Chen, Q., Li, H., Tang, H., Zhang, Y., and Yao, S. Green synthesis of carbon dots with down- and up-conversion fluorescent properties for sensitive detection of hypochlorite with a dual-readout assay. *Analyst,* 138(21):6551-6557, 2013.

[4] Wang, W., Li, Y., Cheng, L., Caob, Z., and Liu, W. Water-soluble and phosphorous-containing carbon dots with strong green fluorescent for cell labeling. *Journal of Materials Chemistry B,* 2(1):46-48, 2014.

[5] Zhou, L., He, B., and Huang, J. Amphibious fluorescent carbon dots: One-step green synthesis and application for light-emitting polymer nanocomposites. C*hemical Communications,* 49(73):8078-8080, 2013.

[6] Gogoi, S., Kumar, M., Mandal, B. B., and Karak, N. High performance luminescent thermosetting waterborne hyperbranched polyurethane/carbon quantum dot nanocomposite with *in vitro* cytocompatibility. *Composite Science and Technol*ogy, 118:39-46, 2015.

[7] De, B., Voit, B., and Karak, N. Transparent luminescent hyperbranched epoxy/carbon oxide dot nanocomposites with outstanding toughness and ductility. *ACS Applied Materials & Interfaces*, 5(20):10027-10034, 2013.

[8] Hao, Y., Gan, Z., Xu, J., Wu, X., and Chu, P. Poly(ethylene glycol)/carbon quantum dot composite solid films exhibiting intense and tunable blue-red emission. *Applied Surface Science*, 311:490-497, 2014.

[9] Parkin, I. P. and Palgrave, R. G. Self cleaning coatings. *Journal of Materials Chemistry*, 15(17):1689-1695, 2005.

[10] Mosconi, D., Mazzier, D., Silvestrini, S., Privitera, A., Marega, C., Franco, L., and Moretto, A. Synthesis and photochemical applications of processable polymers enclosing photoluminescent carbon quantum dots. *ACS Nano*, 9(4):4156-4164, 2015.

[11] Konwar, A., Gogoi, N., Majumdar, G., and Chowdhury, D. Green chitosan-carbon dots nanocomposite hydrogel film with superior properties. *Carbohydrate Polymers*, 115:238-245, 2015.

[12] Zhu, L., Yin, Y., Wang, C. F., and Chen, S. Plant leaf-derived fluorescent carbon dots for sensing, patterning and coding. *Journal of Materials Chemistry C*, 1(32):4925-4932, 2013.

[13] Noguchi, T. and Fujishima, A. Photocatalytic degradation of gaseous formaldehyde using TiO_2 films. *Environmental Sciences & Technology*, 32(23):3831-3833, 1998.

[14] Sun, D., Ban, R., Zhang, P. H., Wu, G. H., Zhang, J. R., and Zhu, J. J. Hair fiber as a precursor for synthesizing of sulfur- and nitrogen-co-doped carbon dots with tunable luminescence properties. *Carbon*, 64:424-434, 2013.

[15] Yang, Z., Xu, M., Liu, M., Liu, Y., He, F., Gao, F., Su, Y., Wei, H., and Zhang, Y. Nitrogen-doped, carbon-rich, highly photoluminescent carbon dots from ammonium citrate. *Nanoscale*, 6(3):1890-1895, 2014.

[16] Li, H., He, X., Kang, Z., Huang, H., Liu, Y., Liu, J., Lian, S., Tsang, C. H. A., Yang, X., and Lee, S. T. Water soluble fluorescent carbon quantum dots and photocatalyst design. *Angewandte Chemie*, 49(26):4430-4434, 2010.

[17] Li, H., Liu, R., Liu, Y., Huang, H., Yu, H., Ming, H., Lian, S., Lee, S. T., and Kang, Z. Carbon dots/Cu_2O composite with protruding nanostructures and their highly efficient (near) infrared photocatalytic behaviour. *Journal of Materials Chemistry*, 22(34):17470-17475, 2012.

[18] Teng, X., Ma, C., Ge, C., Yan, M., Yang, J., Zhang, Y., Moraiscd, P. C., and Bi, H. Green synthesis of nitrogen-doped carbon dots from konjac flower with "off-on" fluorescence by Fe^{3+} and L-lysine for bioimaging. *Journal of Materials Chemistry B*, 2(29):4631-4639, 2014.

[19] Chandra, S., Laha, D., Pramanik, A., Chowdhuri, A. R., Karmakarband, P., and Sahua, S. K. Synthesis of highly fluorescent nitrogen and phosphorous doped carbon dots for the detection of Fe^{3+} ions in cancer cells. *Luminescence*, 31(1):81-87, 2016.

[20] Fernandes, D., Krysmann, M. J., and Kelarakis, A. Carbon dot based nanopowders and their application for fringerprint recovery. *Chemical Communications*, 51(23):4902-4905, 2015.

[21] Ma, Z., Ming, H., Huang, H., Liu, Y., and Kang, Z. One-step ultrasonic synthesis of fluorescent N-doped carbon dots from glucose and their visible-light sensitive photocatalytic ability. *New Journal of Chemistry*, 36(4):861-864, 2012.

[22] Konwar, U. and Karak, N. *Mesua ferra* L. seed oil based highly branched environment friendly polyester resin/clay nanocomposites. *Journal of Polymers and the Environment*, 19(1):90-99, 2011.

[23] Konwar, U., Mandal, M., and Karak, N. *Mesua ferrea* L. seed oil based acrylate-modified thermostable and biodegradable highly branched polyester resin/clay nanocomposites. *Progress in Organic Coatings*, 72(4):676-685, 2011.

[24] Benavides, E. U., Kayatin, M. J., and Davis, V. A. Dispersion and rheology of multiwalled carbon nanotubes in unsaturated polyester resin. *Macromolecules*, 46(4):1642-1650, 2013.

[25] Pramanik, S., Hazarika, J., Kumar, A., and Karak, N. Castor oil based hyperbranched poly(ester amide)/polyaniline nanofiber nanocomposites as antistatic materials. *Industrial & Engineering Chemistry Research*, 52(16):5700-5707, 2013.

[26] Kota, A. K., Cipriano, B. H., Duesterberg, M. K., Gershon, A. L., Powell, D., Raghavan, S. R., and Bruck, H. A. Electrical and rheological percolation in polystyrene/MWCNT nanocomposites. *Macromolecules*, 40(20):7400-7406, 2007.

[27] Madbouly, S. A., Otaigbe, J. U., Nanda, A. K., and Wicks, D. A. Rheological behavior of POSS/polyurethane-urea nanocomposite films prepared by homogeneous solution polymerization in aqueous dispersions. *Macromolecules*, 40(14):4982-4991, 2007.

[28] Yang, J., Han, C. R., Duan, J. F., Xu, F., and Sun, R. C. Mechanical and viscoelastic properties of cellulose nanocrystal reinforced poly(ethylene glycol) nanocomposite hydrogel. *ACS Applied Materials & Interfaces*, 5(8):3199-3207, 2013.

[29] Teng, T. P., Teng, T. C., and Pan, S. Degradation of gaseous formaldehyde by visible light-responsive titania photocatalyst filter. *International Journal of Photoenergy*, 2012:739734(1-10), 2012.

[30] Hazarika, D. and Karak, N. Waterborne sustainable tough hyperbranched aliphatic polyester thermosets. *ACS Sustainable Chemistry & Engineering*, 3(10):2458-2468, 2015.

[31] Zhang, G., Zhang, H., Zhang X., Zhu, S., Zhang, L., Meng, Q., Wang, M., Li, Y., and Yang, B. Embedding graphene nanoparticles into poly (*N,N′*-dimethylacrylamine) to prepare transparent nanocomposite films with high refractive index. *Journal of Materials Chemistry*, 22(39):21218-21224, 2012.

[32] Tome, L. C., Silva, N. H. C. S., Soares, H. R., Coroadinha, A. S., Sadocco, P., Marruchoa, I. M., and Freire, C. S. R. Bioactive transparent films based on polysaccharides and cholinium carboxylate ionic liquids. *Green Chem*istry, 17(8):4291-4299, 2015.

[33] Zhang, H., Zhao, L., Geng, F., Guo, L. H., Wan, B., and Yang, Y. Carbon dots decorated graphitic carbon nitride as an efficient metal-free photocatalyst for phenol degradation. *Applied Catalysis B: Environmental*, 180:656-662, 2016.

[34] Nakata, K., Sakai, M., Ochiai, T. Murakami, T. Takagi, K., and Fujishima, A. Antireflection and self-cleaning properties of a moth-eye-like surface coated with TiO_2 particles. *Langmuir*, 27(7):3275-3278, 2011.

[35] Zhao, J., Liu, F., Wang, G., Cao, T., Guo Z., and Zhang, Y. High performance liquid chromatography determination of formaldehyde in engine exhaust with

unsymmetrical dimethylhydrazine as a new derivatization agent. *Analytical Methods*, 7(1):309-312, 2015.

[36] Mehta, V. N., Jha, S., Basu, H., Singhal, R. K., and Kailasa, S. K. One-step hydrothermal approach to fabricate carbon dots from apple juice for imaging of mycobacterium and fungal cells. *Sensors and Actuators B: Chemical*, 213:434-443, 2015.

[37] Bora, C., Gogoi, P., Baglari, S., and Dolui, S. K. Preparation of polyester resin/graphene oxide nanocomposite with improved mechanical strength. *Journal of Applied Polymer Science*, 129(6):3432-3438, 2013.

[38] Dai, J., Ma, S., Wu, Y., Han, L., Zhang, L., Zhua J., and Liu X. Polyesters derived from itaconic acid for the properties and bio-based content enhancement of soybean oil-based thermosets. *Green Chemistry*, 17(36):2383-2392, 2015.

[39] Djordjevic, I., Choudhury, N. R., Dutta, N. K., and Kumar, S. Synthesis and characterization of novel citric acid-based polyester elastomers. *Polymer*, 50(7):1682-1691, 2009.

[40] Sathiskumar, P. S. and Madras, G. Synthesis, characterization, degradation of biodegradable castor oil based polyesters. *Polymer Degradation and Stability*, 96(9):1695-1704, 2011.

[41] Thakur, S. and Karak, N. Multi-stimuli responsive smart elastomeric hyperbranched polyurethane/reduced graphene oxide nanocomposites. *Journal of Materials Chemistry A*, 2(36):14867-14885, 2014.

[42] Konwar, U. and Karak, N. Epoxy-modified *Mesua Ferrea* L. seed-oil-based polyester/clay nanocomposites. *International Journal of Polymeric Materials and Polymeric biomaterials*, 60(10):799-816, 2011.